

The Soft X-ray Aspect of Gamma-ray Bursts in the Einstein Probe Era

HAO-XUAN GAO,¹ JIN-JUN GENG,^{1,*} YI-FANG LIANG,^{1,2} HUI SUN,³ FAN XU,⁴ XUE-FENG WU,^{1,2,†} YONG-FENG HUANG,^{4,5} ZI-GAO DAI,⁶ AND WEI-MIN YUAN³

¹*Purple Mountain Observatory, Chinese Academy of Sciences, Nanjing 210023, China*

²*School of Astronomy and Space Sciences, University of Science and Technology of China, Hefei 230026, China*

³*National Astronomical Observatories, Chinese Academy of Sciences, Beijing 100101, China*

⁴*School of Astronomy and Space Science, Nanjing University, Nanjing 210023, China*

⁵*Key Laboratory of Modern Astronomy and Astrophysics (Nanjing University), Ministry of Education, China*

⁶*Department of Astronomy, School of Physical Sciences, University of Science and Technology of China, Hefei 230026, China*

ABSTRACT

The Einstein Probe (EP) satellite, dedicated at time-domain high-energy astrophysics and multi-messenger astronomy, was recently launched and successfully put into operation. The wide-field X-ray telescope (WXT, 0.5-4 keV) onboard has identified multiple gamma-ray burst (GRB) events, with an average duration of several hundred seconds. This duration is several times longer than the average duration of long gamma-ray bursts (LGRBs) detected by the Neil Gehrels *Swift* Observatory, which typically stands at several tens of seconds. Additionally, EP has detected some unknown X-ray transients whose connection to GRBs is uncertain, due to the absence of gamma-ray counterparts and efficient follow-up observation at multi-wavelengths. Several main factors could account for the longer time, including the Doppler effect of off-axis viewing, the spectral lag effect of the synchrotron spectrum of cooling electrons, and some unknown prolonged intrinsic X-ray activities. Our studies indicate that EP GRBs may primarily consist of off-axis viewed bursts, forming a unique population among the GRB zoo, yet the intrinsic origin for the specific bursts could not be excluded. By analyzing the statistical properties of the historical LGRB samples, we explored observable properties of on-axis and off-axis LGRBs in the soft X-ray band. The predicted characteristics of off-axis viewed GRBs, including the duration, energy fluence, low-energy spectral index, and the slopes of Amati and Yonetoku relations, could be tested with a larger sample of GRB events detected by EP in the future.

1. INTRODUCTION

Gamma-ray bursts (GRBs), the most energetic stellar explosions in the Universe, have been observed and studied for nearly 60 years. The prompt emission of GRBs is thought to come from the relativistic jet launched from the central compact remnant (Blandford & Znajek 1977; Eichler et al. 1989; Piran 2004; Kumar & Zhang 2015). It typically lasts for a few seconds (or less) and has a variable light curve consisting of several spikes. However, the radiation mechanism responsible for the prompt emission remains an open question (Zhang 2018). Both synchrotron radiation of non-thermal electrons (e.g., Mészáros et al. 1994; Tavani 1996; Zhang & Yan 2011a) and photospheric emission (e.g., Rees & Mészáros 2005; Pe'er et al. 2006; Ryde et al. 2011) have been proposed to explain the GRB prompt emission. Recently, Burgess et al. (2020) suggest that synchrotron spectra from electrons in evolving (fast-to-slow) cooling regimes

are capable of fitting 95% of all time-resolved spectra of the brightest long GRBs observed by the gamma-ray burst monitor (GBM: 8 keV-40 MeV) on board the NASA *Fermi* Gamma-Ray Observatory by comparing the theoretical results with observed data directly.

Before a relativistic outflow launched by the central engine can produce a successful GRB, it would inevitably propagate through the envelope or the ejected materials of the progenitor star (Bromberg et al. 2011; Berger 2014; Nagakura et al. 2014; Nakar & Piran 2016). The structure of the jet may result from the jet formation mechanism itself (van Putten & Levinson 2003; Vlahakis et al. 2003; Aloy et al. 2005), or it may arise from the breakout process as the jet penetrates the stellar materials (Levinson & Eichler 2003; Zhang et al. 2003; Lazzati 2005; Morsanyi et al. 2010; Pescall et al. 2015; Geng et al. 2016b). Structured jets, characterized by a narrow, highly relativistic inner core surrounded by less energetic, slower-moving wings at larger angles, have been extensively studied in the GRB community for over 20 years (e.g., Mészáros et al. 1998; Dai & Lu 2001; Lipunov et al. 2001; Zhang & Mészáros 2002a; Rossi et al. 2002; Kumar &

* E-mail: jjgeng@pmo.ac.cn

† E-mail: xfwu@pmo.ac.cn

Granot 2003). Two main types of structured jets, i.e., power-law like and Gaussian like jets, have have been discussed in the literature (Granot et al. 2017; Lazzati et al. 2018; Troja et al. 2019; Ryan et al. 2020; Lamb & Kobayashi 2017; Xiao et al. 2017; Kathirgamaraju et al. 2018; Meng et al. 2018; Geng et al. 2019; Li et al. 2019; Gao et al. 2022; O'Connor et al. 2024).

The duration of a burst is usually defined by the so-called “ T_{90} ”, which is the time interval from 5 per cent to 95 per cent of the accumulated fluence. It is found that the distribution of T_{90} shows two Gaussian components with a separation line around 2 seconds in the logarithmic space (Meegan et al. 1992; Kouveliotou et al. 1993). These two components are nowadays commonly classified into the short ($T_{90} < 2$ s) and long ($T_{90} > 2$ s) classes, which are widely believed to originate from relativistic outflows ejected during the merger of binary compact stars and the collapse of massive stars, respectively. The number ratio of the two classes and the peak duration values of them are dependent on the energy bands and sensitivities of the instruments (e.g. Kouveliotou et al. 1993; Sakamoto et al. 2008, 2011; Paciesas & Fermi GBM Collaboration 2012; Zhang et al. 2012; Qin & Chen 2013).

On the other hand, the cosmic rate and the luminosity function (LF) of GRBs allows us to test theories about their progenitors (e.g. Liang et al. 2007; Pescalli et al. 2015). These two functions have been derived for the population of long GRBs using various methods and samples of bursts (e.g. Daigne et al. 2006; Guetta & Della Valle 2007; Firmani et al. 2004; Salvaterra & Chincarini 2007; Salvaterra et al. 2009, 2012; Wanderman & Piran 2010; Yu et al. 2015; Petrosian et al. 2015; Lan et al. 2021). Given the incomplete sampling of faint bursts and the low completeness in redshift measurements, Lan et al. (2021) carefully selected a subsample of bright *Swift* bursts to revisit the GRB LF and redshift distribution, accounting for the probability of redshift measurement. They also explored two general forms for the GRB LF: a broken power-law LF and a triple power-law LF. Their results indicate that strong redshift evolution, either in luminosity (with an evolution index of $\delta = 1.92^{+0.25}_{-0.37}$) or in density ($\delta = 1.26^{+0.33}_{-0.34}$), is necessary to adequately explain the observations, regardless of the assumed form of the GRB LF.

The spectrum of the prompt emission is non-thermal and often described by the so-called Band function empirically (Band et al. 1993). The Band function is characterized by three parameters, the low-energy and high-energy photon spectral indices and the peak energy (E_p). In past years, significant efforts have been dedicated to model the shape of prompt emission spectra (e.g., Mészáros & Rees 2000; Pe'er et al. 2006; Beloborodov 2010; Uhm & Zhang 2014, 2016; Uhm et al. 2018; Geng et al. 2018b; Gao et al. 2021). GRBs display correlations between the peak energy and other observational parameters. The most famous one is the Amati

relation (Amati et al. 2002). It connects the intrinsic hardness of $E_{p,z}$, calculated as $E_{p,z} = E_p(1+z)$, and the isotropic equivalent total energy of $E_{\gamma,\text{iso}}$ emitted in gamma-rays within the 1 to 10^4 keV range. The index of the Amati relation is about 0.5 (Amati 2006; Nava et al. 2012; Demianski et al. 2017; Minaev & Pozanenko 2020). Another important relation, the Yonetoku relation (Yonetoku et al. 2004), shows the correlation between the intrinsic hardness of $E_{p,z}$ and the peak luminosity of $L_{p,\text{iso}}$. The physical origin of these empirical relations remain under debate. Some researchers have attempted to derive the on-axis and off-axis Amati relation indices by the analytical method or by means of numerical calculations (Zhang & Mészáros 2002b; Granot et al. 2002; Eichler & Levinson 2004; Ramirez-Ruiz et al. 2005; Dado & Dar 2012; Yamazaki et al. 2004; Kocevski 2012; Mochkovitch & Nava 2015; Xu et al. 2023). Xu et al. (2023) provided a simple analytical derivation for both the Amati and Yonetoku relations within the standard fireball model, and this derivation was confirmed by numerical simulations. It was found that these relations strongly depend on the difference between the viewing angle and the jet opening angle when the jet is viewed off-axis.

Recently, the Einstein Probe (EP)¹ satellite, a mission by the Chinese Academy of Sciences (CAS) dedicated at time-domain high-energy astrophysics and multi-messenger astronomy, was launched and successfully put into operation (Yuan et al. 2022, 2024). The mission's primary goals are to discover high-energy transients and monitor variable objects in the soft X-ray band, with sensitivity more than an order of magnitude greater than that of current orbiting instruments. The EP is equipped with two scientific instruments: the wide-field X-ray telescope (WXT, 0.5-4 keV) and the follow-up X-ray telescope (FXT, 0.3-10 keV). The WXT is designed to capture transients and monitor variable objects, while the FXT will perform deep follow-up observations of intriguing targets identified by the WXT and other facilities. The successful operation of EP is expected to generate a wealth of observational data, including soft X-ray emissions during the main burst phase of gamma-ray bursts (GRBs), X-ray-rich GRBs that gamma-ray detectors may miss, and high-redshift GRBs.

EP has detected some GRB events, of which the average duration is approximately several hundred seconds (Yin et al. 2024; Zhang et al. 2024b; Zhou et al. 2024a,b). In contrast, previous studies on the duration of long bursts have shown that the average T_{90} duration of LGRBs is approximately several tens of seconds, while the duration is known

¹ Einstein Probe is an international mission led by the Chinese Academy of Sciences (CAS) in collaboration with the European Space Agency (ESA), the Max-Planck-Institute for extraterrestrial Physics (MPE), Germany, and the Centre National d'Études Spatiales (CNES), France.

to be energy-dependent (Qin & Chen 2013). Additionally, EP has detected some unknown X-ray transients that may be related to GRBs, but uncertain due to the absence of gamma-ray counterparts and efficient follow-up observation at multi-wavelengths. These transients also have long durations, such as EP240414a and EP240416a (Lian et al. 2024a; Cheng et al. 2024). It may indicate that a considerable sample of underlying LGRBs have relatively longer duration in the soft X-ray band, and point to the possibility of a distinct population among GRBs.

There are three possible origins of EP GRBs. First, EP GRBs may consist of off-axis viewed LGRBs (Troja et al. 2017; Granot et al. 2017; Haggard et al. 2017; Ioka & Nakamura 2018). Due to the Doppler effect, off-axis LGRBs can exhibit longer durations compared to those of on-axis LGRBs. The radiation energy of these bursts is concentrated in the soft X-ray energy band, while their hard X-ray emission may fall below the detection thresholds of other instruments. This could explain the presence of unidentified X-ray transients with long durations detected by EP. The second possibility comes from the so called “spectral lag” effect, i.e., the observed pulse gets increasingly broader in lower energy band (Cheng et al. 1995; Norris et al. 1996; Band 1997; Norris et al. 2000; Wu & Fenimore 2000; Liang et al. 2006). As a result, LGRBs observed by EP in the soft X-ray band may appear to have longer durations than their counterparts in the hard X-ray band. An alternative possibility is that EP are detecting bursts with some prolonged X-ray activities, potentially induced by the some energy release processes of the central engine, which remains highly uncertain. In this work, we focus on the two former origins. The proportions of on-axis and off-axis bursts in EP-detected GRBs could be estimated through theoretical simulations, helping to distinguish between the two explanations.

In order to examine these two scenarios, we investigate the properties of LGRBs in the soft X-ray band from 0.5 to 4 keV that covers the energy band of EP-WXT. A brief overview of GRBs detected by EP is provided in Section 2. Several statistical characteristics of on-axis LGRBs are reviewed in Section 3. The synchrotron radiation scenario and jet structure adopted in our calculations are briefly described in Section 4. In Section 5, the model parameters are constrained by matching the simulation results with the observed characteristics of on-axis GRBs, including the Amati and Yonetoku relations, the T_{90} duration, and the redshift and luminosity distribution. In Section 6, we derive the properties of several observables for GRBs detected by EP and estimate the proportions of on-axis and off-axis bursts among the EP-detected GRBs. Finally, we summarize our study in Section 7. Throughout this paper a flat Lambda cold dark matter cosmological model with $H_0 = 70 \text{ km s}^{-1} \text{ Mpc}^{-1}$, $\Omega_m = 0.3$, and $\Omega_\Lambda = 0.7$ is adopted.

2. A GLANCE OF EP GRBS

By December 2024, WXT has detected around 11 X-ray transients with GRB origin as being consistent with the detections of the gamma-ray detectors. The first GRB detected by WXT, EP240219a, has a T_{90} duration of approximately 130 seconds in the 0.5-4 keV energy band (Yin et al. 2024). The second GRB observed by WXT, EP240315a, exhibited a T_{90} duration of approximately 1,000 seconds within the same energy band (Liu et al. 2024a). The durations of other 9 GRBs can be collected from the General Coordinates Network (GCN) (Zhang et al. 2024b; Zhou et al. 2024a,b; Fu et al. 2024; Li et al. 2024a,b; Tian et al. 2024; Liu et al. 2024b; Hu et al. 2024b). Additionally, we gathered duration information from GCN for 29 fast X-ray transients detected by WXT, the origins of which remain unknown (Hu et al. 2024a,d,c; Cheng et al. 2024; Pan et al. 2024; Wu et al. 2024; Zhang et al. 2024a; Wang et al. 2024; Yang et al. 2024a,b; Lian et al. 2024b; Peng et al. 2024; Zhang et al. 2024c; Liang et al. 2024). We also collected durations of Fermi GRBs from von Kienlin et al. (2020). A total of 1964 long GRBs were selected based on the criterion that the T_{90} duration of the burst exceeds 2 seconds. The durations in the observer frame of Fermi GRBs, EP GRBs, and fast X-ray transients with unknown origins are presented in Figure 1. The distributions of EP GRBs and unidentified fast X-ray transients are general distributions derived from the GCN data. The average duration of GRBs detected by EP is approximately 280 s, significantly longer than the average duration of ~ 30 s for GRBs observed by Fermi. Notably, fast X-ray transients with unknown origins exhibit a duration distribution similar to that of GRBs detected by EP, with an average duration of approximately 270 s.

The isotropic energies and redshifts of EP GRBs can also be found from GCN. Five GRBs with redshift measurements have been reported: EP240315a, EP240801a, EP241025a, EP241026a, and EP241030a (Liu et al. 2024a; Zheng et al. 2024; Svinkin et al. 2024; Izzo et al. 2024; Li et al. 2024c). Their redshifts range from 1.411 to 4.859. The isotropic energy in the 1-10,000 keV band for EP240315a is 6.4×10^{53} erg (Liu et al. 2024a). The isotropic energies in the 10-10,000 keV band for EP241025a and EP241030a are 5.5×10^{53} erg and 2.8×10^{53} erg, respectively (Svinkin et al. 2024; Ridnaia et al. 2024).

3. THE CHARACTERISTICS OF ON-AXIS LGRBS

Here, we provide a concise overview of the observational properties of LGRBs, which are assumed to be on-axis viewed bursts, including the luminosity and redshift distributions, T_{90} durations, as well as Amati and Yonetoku relations. A detailed description of replicating these characteristics is arranged in Section 5, while the plausible probability distributions of model parameters are determined.

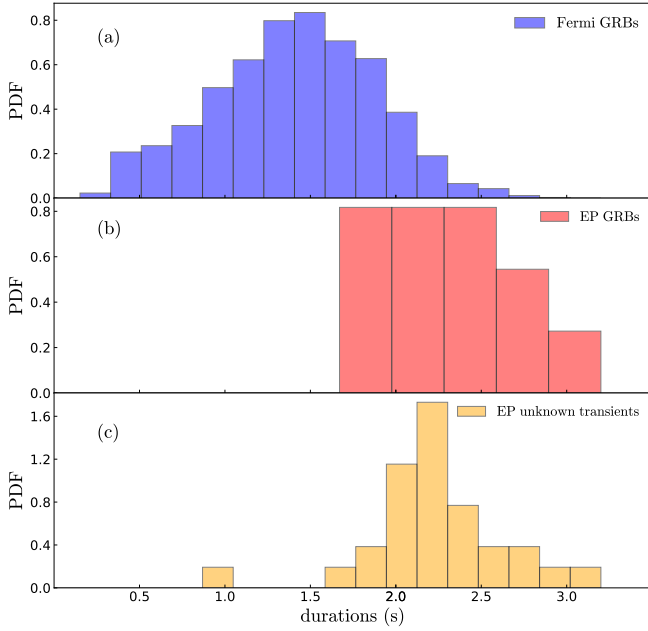


Figure 1. The duration distributions in the observer frame of Fermi GRBs, EP GRBs, and fast X-ray transients of unknown origin are compared. Panel (a) illustrates the duration distribution of 1,964 Fermi LGRBs observed within the 50-300 keV energy band. Panel (b) displays the duration distribution of 11 EP GRBs within the 0.5-4 keV energy band. Panel (c) presents the duration distribution of 29 EP fast X-ray transients of unknown origin, also within the 0.5-4 keV energy band.

3.1. The luminosity and redshift distributions of LGRBs

In the luminosity evolution model, the joint distribution function of redshift (z) and luminosity (L) for LGRBs detected by *Swift*/BAT writes as (Lan et al. 2021)

$$f(L, z) = \frac{1}{N_{\text{exp}}} \frac{c}{H_0} \frac{D_L^2(z)}{\sqrt{\Omega_\Lambda + \Omega_m(1+z)^3}} \Theta(P(L, z)) \times \frac{\psi(z)}{1+z} \phi(L, z), \quad (1)$$

where c is the speed of light, $D_L(z)$ is the luminosity distance at z , $\Theta(P)$ represents the detection efficiency, $P(L, z)$ is the peak flux of the burst, $\psi(z)$ denotes the comoving event rate of GRBs in units of $\text{Mpc}^{-3} \text{yr}^{-1}$, $\phi(L, z)$ is the normalized GRB luminosity function, and detailed function forms of $\Theta(P)$, $P(L, z)$, $\psi(z)$, and $\phi(L, z)$ could be found in Lan et al. (2021). The expected number of GRBs, N_{exp} , is then given by

$$N_{\text{exp}} = \frac{\Delta\Omega T}{4\pi} \int_0^{z_{\text{max}}} \int_{\max[L_{\text{min}}, L_{\text{lim}}(z)]}^{L_{\text{max}}} \Theta(P(L, z)) \frac{\psi(z)}{1+z} \times \phi(L, z) dL dV(z), \quad (2)$$

where $\Delta\Omega$ is the *Swift*/BAT field of view, T is the time of activity of *Swift* that covers the sample, L_{min} and L_{max} are the

minimum and maximum of the luminosity, z_{max} is the maximum redshift, $dV(z)$ is the comoving volume element, $L_{\text{lim}}(z)$ is luminosity threshold determined by the burst redshift and BAT's flux limit, and the detailed values and expressions of them could be found in Lan et al. (2021).

3.2. The detected T_{90} distribution of LGRBs

Horváth & Tóth (2016) collected 997 GRBs from *Swift*/BAT (15-150 keV) and analyzed the $\log T_{90}$ distribution of these bursts in the observer frame using various fitting functions. The two log-normal functions are applicable and are adopted in this paper. For the LGRBs component we are interested in, the function is $N(\mu, \sigma^2)$, with $\mu = 1.70$ and $\sigma = 0.48$.

3.3. The Amati relation and Yonetoku relation

Tsvetkova et al. (2017) presented a catalog of GRBs with known redshifts detected by the Konus-Wind (KW) experiment between 1997 and 2016. They analyzed the distribution of rest-frame GRB parameters and confirmed the Amati and Yonetoku relations for LGRBs. Further, Tsvetkova et al. (2021) reported the results of a systematic study of GRBs with reliable redshift estimates detected simultaneously by the KW experiment (in waiting mode) and the *Swift*/BAT telescope from January 2005 to the end of 2018. In this work, 167 weak and relatively soft GRBs were added to the sample, extending the KW GRBs with known redshifts to a total of 338. The data from this expanded sample were used to fit the parameters of the Amati and Yonetoku relations for LGRBs using a Bayesian method. The derived power-law indices of the Amati and Yonetoku relations for these GRBs are 0.481 and 0.428, respectively.

4. THE MODEL OF GRB JETS

A GRB jet will experience internal energy dissipation, caused by internal shocks resulting from the collision between different outflow parts (Rees & Mészáros 1994; Paczynski & Xu 1994) or magnetic reconnection (Spruit et al. 2001; Zhang & Yan 2011b). Meanwhile, the electrons in the jet can be accelerated and form a non-thermal distribution in the energy space. The distribution of accelerated electrons is assumed to be a power-law of $Q(\gamma'_e, t') = Q_0(t')(\gamma'_e/\gamma'_m)^{-p}$ for $\gamma'_e > \gamma'_m$, where Q_0 is related to the injection rate by $N'_{\text{inj}} = \int_{\gamma'_m}^{\gamma'_{\text{max}}} Q(\gamma'_e, t') d\gamma'_e$ ² (the superscript prime ' denotes the quantities in the comoving frame hereafter). These electrons will lose their energy owing to the synchrotron radiation and adiabatic cooling. Therefore, their energy distribution shows a time evolution, which is described by the continuity equa-

² γ'_{max} is the maximum Lorentz factor of electrons and is given by the approximation $\gamma'_{\text{max}} \simeq 10^8 \left(\frac{B}{G}\right)^{-0.5}$ (Huang et al. 2000).

tion (Uhm & Zhang 2014; Geng et al. 2018b; Zhang et al. 2019; Gao et al. 2021; Gao et al. 2024) of

$$\frac{\partial}{\partial t'} \left(\frac{dN_e}{d\gamma'_e} \right) + \frac{\partial}{\partial \gamma'_e} \left[\dot{\gamma}'_{e,\text{tot}} \left(\frac{dN_e}{d\gamma'_e} \right) \right] = Q(\gamma'_e, t'). \quad (3)$$

As the GRB jet rapidly expands with a bulk Lorentz factor of Γ , the toroidal-dominated magnetic field in the comoving frame decreases as $B' = B'_0(R/R_0)^{-q}$ (Uhm & Zhang 2014), where R_0 is the radius where the jet begins to produce photons and R is the radius of the expanding shell. The non-thermal electrons will be scattered by the magnetic field and emit photons with the synchrotron radiation power of P'_{syn} (Rybicki & Lightman 1979). The observed emission originates from jet elements at various latitudes, assuming a power-law structured jet described by

$$\begin{aligned} \frac{dL}{d\Omega} &= \begin{cases} L_c, & \theta \leq \theta_c, \\ L_c (\theta/\theta_c)^{-k_L}, & \theta_c < \theta \leq \theta_m, \end{cases} \\ \frac{d\Gamma}{d\Omega} &= \begin{cases} \Gamma_c, & \theta \leq \theta_c, \\ \Gamma_c (\theta/\theta_c)^{-k_\Gamma} + 1, & \theta_c < \theta \leq \theta_m, \end{cases} \end{aligned} \quad (4)$$

where L_c and Γ_c are the luminosity and the Lorentz factor of the inner core, respectively. θ_m is the maximum of the half-opening angle. The indices k_L and k_Γ describe the angular distribution of luminosity density $L(\theta)$ and Lorentz factor $\Gamma(\theta)$ within the jet cone. Note that to obtain the observed spectral flux, $F_{\nu_{\text{obs}}}$, it is necessary to sum up the emission from electrons over the equal-arrival-time surface (Geng et al. 2016a):

$$F_{\nu_{\text{obs}}} = \frac{1+z}{4\pi D_L^2} \int_0^{\theta_m} P'_{\text{syn}}(\nu'(\nu_{\text{obs}})) \mathcal{D}^3 \frac{\sin \theta}{2} d\theta. \quad (5)$$

5. MONTE CARLO SIMULATIONS

The synchrotron radiation scenario is expected to reproduce the empirical distributions and relations mentioned in Section 3. To test this idea, Monte Carlo simulations were performed. These simulations involve seven input parameters: Γ_c , γ'_m , N'_{inj} , B'_0 , R_0 , t_{off} , and z . Here, t_{off} denotes the time in the observer frame at which electron injection ceases. In this paper, we define a burst as an on-axis GRB if the viewing angle is less than the core angle of the GRB jet, and as an off-axis GRB if the viewing angle is greater than the core angle. In our simulations, the core angle, θ_c , is assumed to follow a normal Gaussian distribution of $N(2.5^\circ, 1^\circ)$ (Wang et al. 2018), the power-law index of accelerated electrons is set to $p = 2.3$, the parameter q is fixed at $q = 1$, the θ_m is set to $10\theta_c$. We assume that an on-axis observer's line of sight has an equal probability of pointing to any direction within the solid angle defined by the range of $[0, \theta_c]$, which can be expressed as

$$\frac{dP}{\sin \theta_v d\theta_v d\phi} = \frac{1}{\int_0^{2\pi} \int_0^{\theta_c} \sin \theta_v d\theta_v d\phi}, \quad (6)$$

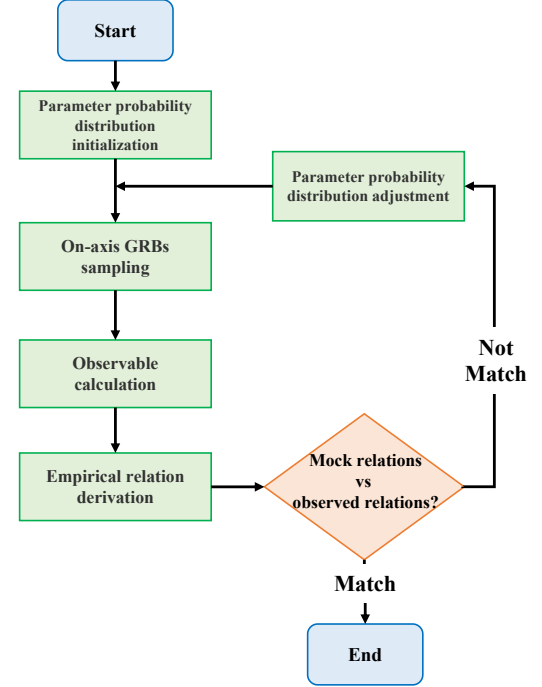


Figure 2. The flow chart for replicating statistical characteristics of on-axis LGRBs.

where θ_v and ϕ represent the viewing angle and azimuthal angle, respectively, measured relative to the jet central axis. In this section, the parameters k_L and k_Γ are fixed at 2 to replicate statistical characteristics of on-axis LGRBs. The assumptions for these relevant parameters are summarized in Table 1.

Given the substantial computational cost of each calculation and the potential for strong parameter degeneracies, we did not employ a rigorous Bayesian method for parameter constraint in this study. Instead, we manually adjusted the probability distribution of physical parameters until a satisfactory visual agreement was achieved between the simulation outcomes and the observed empirical relations. Additionally, observational data indicate that approximately 80% of GRBs display prompt emission signatures composed of a single emission episode (Koshut et al. 1995; Lazzati 2005; Burlon et al. 2008; Bernardini et al. 2013; Hu et al. 2014; Lan et al. 2018). To streamline the simulation process, we modeled long-duration bursts as consisting of a single episode with one pulse, even though multiple pulses may be present within a single episode (Lu et al. 2012).

The simulation process (also shown in Figure 2) is as follows:

1. Generation of Input Parameters: Assuming that key parameters follow specific distributions, a set of seven input parameters are randomly generated. Each set of parameters define a mock GRB.

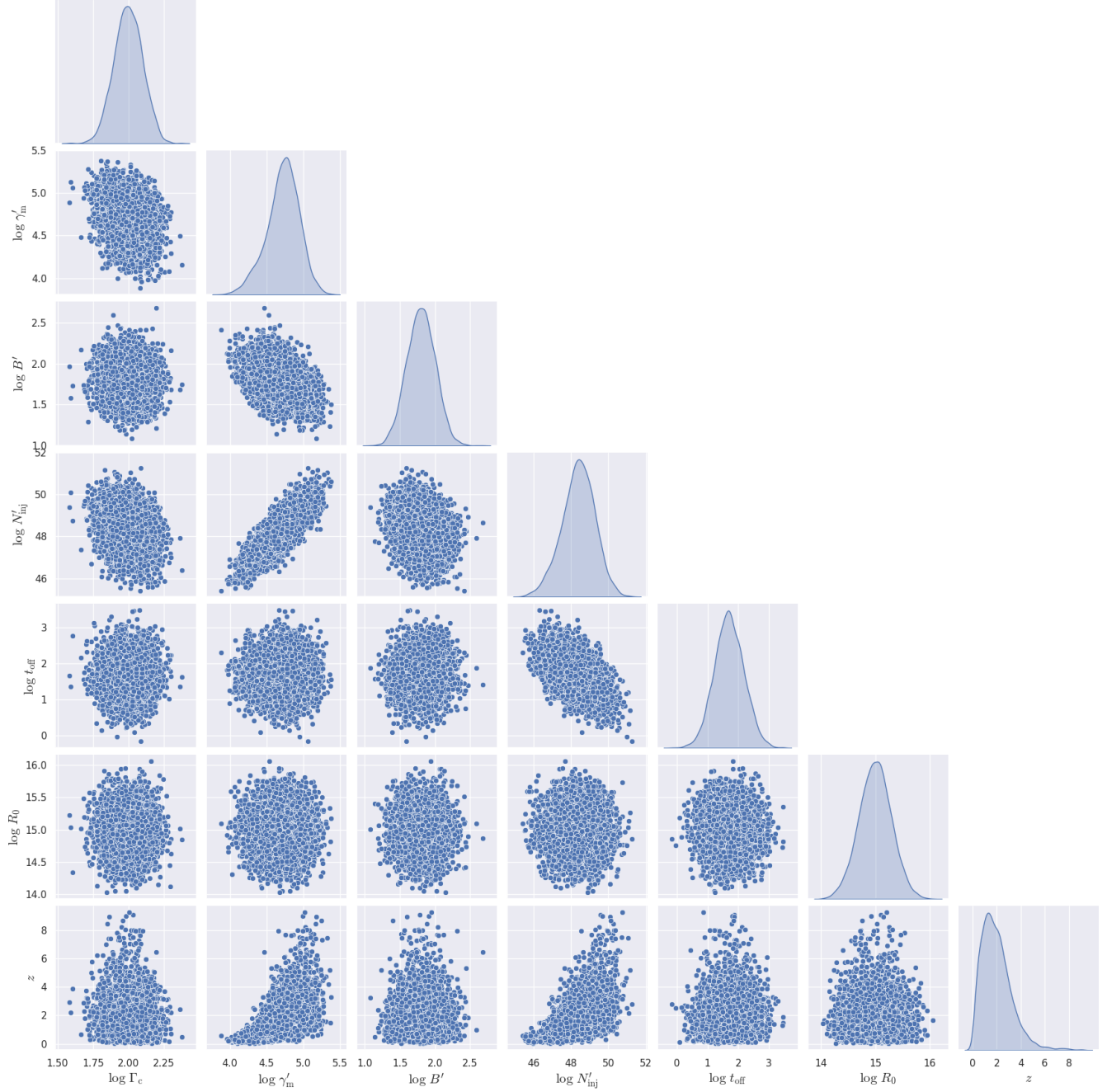


Figure 3. The optimal probability distribution of model input parameters, including Γ_c , γ'_m , N'_{inj} , B'_0 , R_0 , t_{off} , and z .

Table 1. Assumptions of relevant parameters in simulations for on-axis and off-axis bursts.

Burst	θ_c	θ_m	θ_v	p	q	k_L	k_Γ
On-axis	$N(2.5^\circ, 1^\circ)$	$10\theta_c$	$\leq \theta_c$	2.3	1	2	2
Off-axis	$N(2.5^\circ, 1^\circ)$	$10\theta_c$	$> \theta_c$	2.3	1	$U(2, 4)$	$U(2, 4)$

NOTE—The normal Gaussian distribution is denoted by $N(\mu, \sigma)$, while the uniform distribution is represented by $U(a, b)$.

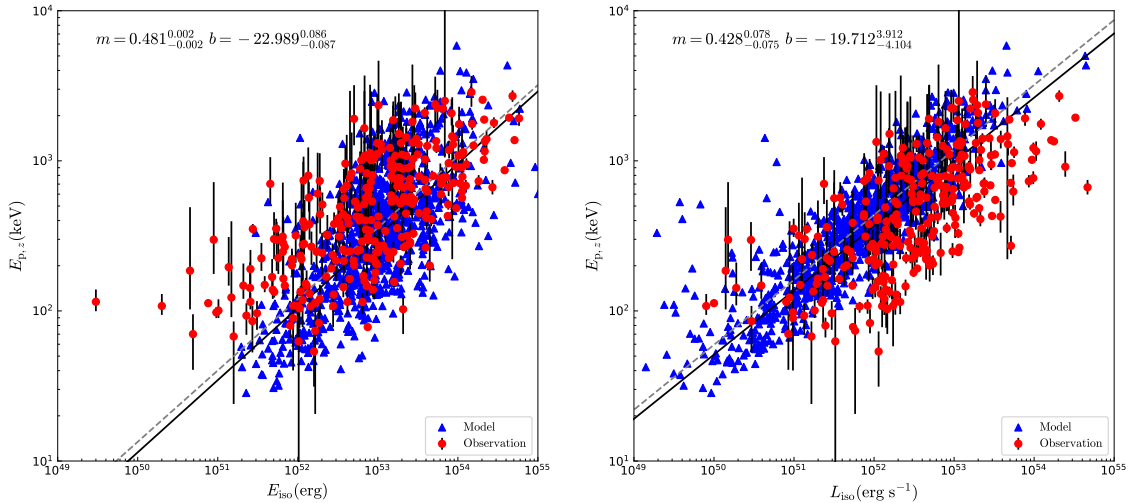


Figure 4. The distribution of mock and observed LGRBs in the $L_{p,\text{iso}}-E_{p,z}$ and $E_{y,\text{iso}}-E_{p,z}$ planes. The red circle dots represent observed LGRBs from Tsvetkova et al. (2021), and the blue triangular dots show our mock results for on-axis LGRBs. The solid line and the dashed line correspond to the best-fit result for observed and mock samples, respectively.

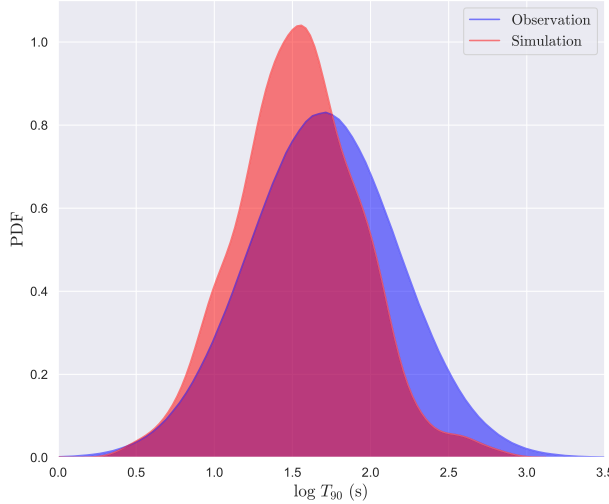


Figure 5. The probability distribution of $\log T_{90}$ duration in the observer frame for both mock and observed LGRBs in the hard X-ray band.

The blue and red shadows represent observed LGRBs from Horváth & Tóth (2016) and mock GRBs, respectively.

2. Numerical Calculation: The model is then applied to numerically calculate the corresponding values of E_p , $E_{\gamma, \text{iso}}$, and $L_{p, \text{iso}}$ for the mock GRB.

3. Sample Creation: Steps 1 and 2 are repeated to create a large sample containing 1,000 GRBs.

4. Empirical Relations: The empirical relations or distributions for the mock GRBs are derived using the Bayesian method.

5. Probability Distribution Adjustment: The empirical relations of the mock GRBs are compared with the observed empirical relations. Based on these comparisons, the initial probability distributions of input parameters are adjusted to better match the observational relations.

These five steps are repeated iteratively until the empirical relations of the mock GRBs closely align with those determined by the observation. Through this iterative process, plausible probability distributions of input parameters for the synchrotron emission scenario are determined.

5.1. The generation of input parameters

In this subsection, we constrain our model parameters using the observational properties of LGRBs outlined in Section 3. The GRB spectrum, characterized by a Band function $N(E)$ with typical low-energy and high-energy spectral indices of $\alpha_s = -1.5$ and $\beta_s = -2.3$ (Band et al. 1993; Preece et al. 2000; Kaneko et al. 2006), is also incorporated into the parameter constraint process. We assume the seven physical parameters in the model are governed by four key observational constraints. First, the observed T_{90} distribution of LGRBs constrains the injection timescale of

shock-accelerated electrons. Second, Equation (1) governs the redshift distribution of bursts and encodes the redshift-luminosity correlation. Additionally, Equation (7) links the burst luminosity to the spectral peak energy. These constraints collectively imply that only three parameters can be independently assigned median values under our assumption of log-normal probability distributions for the parameters.

To streamline parameter constraints, we adopt the following strategy:

1. The redshift z is sampled directly from the probability distribution in Equation (1).

2. The parameter t_{off} , which approximately represents the duration of the burst, is sampled from observed T_{90} distribution of LGRBs (Subsection 3.2).

3. The bulk Lorentz factor (Γ_c), magnetic field strength (B'_0), and jet radius (R_0) are assumed to follow log-normal distributions, with their logarithmic values drawn from $N(\mu, \sigma^2)$.

4. The remaining parameters, the injected rate of electrons N'_{inj} and the minimum electron Lorentz factor γ'_m , are derived analytically using the Yonetoku correlation rather than assuming log-normal priors. The mock GRB distribution is then calibrated by iteratively adjusting the medians and variances of Γ_c , B'_0 , and R_0 until consistency with observations is achieved. Below, we detail the derivation of γ'_m and N'_{inj} from the other parameters.

The parameters γ'_m and N'_{inj} are connected to the peak energy and the spectral morphology. The peak energy E_p can always be estimated using the empirical Yonetoku correlation of

$$E_p(1+z)/\text{keV} = C(L_{p, \text{iso}}/\text{erg})^{0.428}, \quad (7)$$

where the constant of C equals $10^{-19.712}$, which is determined by fitting observation data of Tsvetkova et al. (2021). The redshift z and isotropic peak luminosity $L_{p, \text{iso}}$ are generated via Monte Carlo sampling based on Equation (1). Then the minimum electron Lorentz factor γ'_m , governed by synchrotron radiation physics and Doppler boosting, is derived from (Geng et al. 2018b)

$$\gamma'_m = \sqrt{\frac{4\pi m_e c(1+z)E_p}{3hq_e B'_0 \Gamma_c}}, \quad (8)$$

where h , m_e , and q_e denote the Planck constant, electron rest mass, and electron charge. The peak specific flux $F_{\nu_{\text{obs}}}(\nu_p)$, determined by GRB spectral properties, is expressed as

$$F_{\nu_{\text{obs}}}(\nu_p) = A h E_p N(E_p), \quad (9)$$

where $\nu_p = E_p/h$ and $A = L_{p, \text{iso}}/4\pi D_L^2 / \int_{1/(1+z)}^{10^4/(1+z)} EN(E)dE$.

Then the electron injection rate can be derived from

$$N'_{\text{inj}} = F_{\nu_{\text{obs}}}(\nu_p) \frac{\sigma_T c B'_0 \gamma'_m}{\sqrt{3} q_e^3 \Gamma_c} \frac{2D_L^2}{3(1+z)}. \quad (10)$$

where σ_T is the Thomson cross-section.

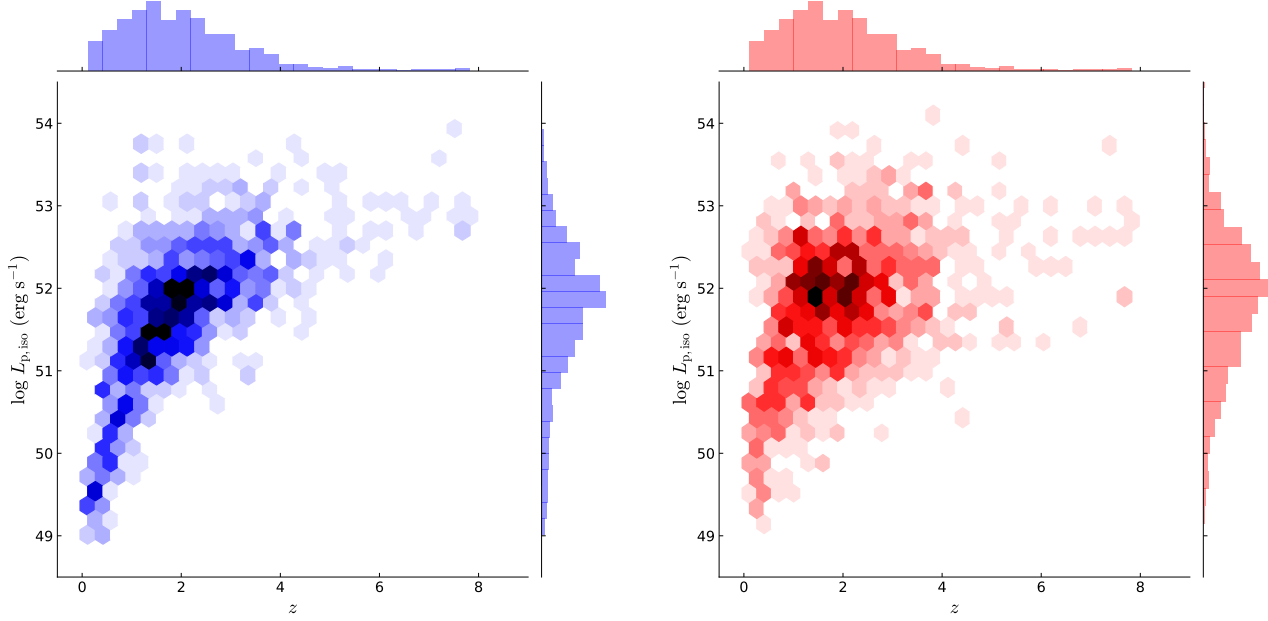


Figure 6. The left and right panels show the probability distribution of redshift and luminosity for observed GRBs and mock LGRBs, respectively.

5.2. The generation of observables

For each group of input parameters, the isotropic bolometric emission energy, the bolometric peak luminosity, the peak energy of the time-integrated spectrum, and the T_{90} duration in the hard X-ray band are calculated. The isotropic emission energy is defined as (Bloom et al. 2001)

$$E_{\gamma,\text{iso}} = \frac{4\pi D_L^2 \int_0^{\Delta T} dt_{\text{obs}} \int_{\nu_1/(1+z)}^{\nu_2/(1+z)} F_{\nu_{\text{obs}}} d\nu_{\text{obs}}}{1+z}, \quad (11)$$

where ΔT is the time during which the observed γ -ray flux surpasses the detection threshold ($\sim 2 \times 10^{-8}$ erg cm $^{-2}$ s $^{-1}$) of the *Swift*/BAT, with an exposure time set at 2 seconds. The frequencies ν_1 and ν_2 correspond to the frequencies of the 10 keV and 10^4 keV photons, respectively. The bolometric peak luminosity $L_{\text{p,iso}}$ is the peak value of the isotropic emission luminosity L given by

$$L = 4\pi D_L^2 \int_{\nu_1/(1+z)}^{\nu_2/(1+z)} F_{\nu_{\text{obs}}} d\nu_{\text{obs}}. \quad (12)$$

The peak energy, E_p , of the time-integrated spectrum is obtained by fitting the time-integrated flux $\int_0^{\Delta T} F_{\nu_{\text{obs}}} dt_{\text{obs}}$ with the Band function. To compute the T_{90} duration, we calculate the photon count spectrum by using $C(\nu_{\text{obs}}) = \frac{F_{\nu_{\text{obs}}}}{h\nu_{\text{obs}}}$, where the unit of $C(\nu_{\text{obs}})$ is cts \cdot s $^{-1}$ \cdot Hz $^{-1}$. T_{90} is defined by the time interval between the epochs when 5% and 9% of the total fluence collected by the detector and can be expressed as

$$T_{90} = t_{95} - t_5. \quad (13)$$

5.3. The optimal probability distribution of input parameters

After numerous iterations, we identified the optimal probability distribution of input parameters, which are illustrated in Figure 3. The corresponding probability distributions of the mock GRBs are presented in Figures 4-6. As shown in Figure 4, the distribution of mock GRBs in the $L_{\text{p,iso}}\text{-}E_{\text{p,z}}$ and $E_{\gamma,\text{iso}}\text{-}E_{\text{p,z}}$ planes aligns well with those of the observed LGRBs. The slopes of Amati and Yonetoku relations for mock GRBs are 0.475 and 0.434, which are close to the corresponding slope values of 0.481 and 0.428 of the observed LGRBs. The probability distribution of the T_{90} duration in the hard X-ray band for mock GRBs is exhibited in Figure 5. The average T_{90} duration for mock GRBs is about 40 s, which is close to the observed average value of ~ 50 s for LGRBs. A comparison of the probability distributions of redshift and luminosity between the mock LGRBs and the observed LGRBs is shown in Figure 6. Although the median luminosity of the mock GRBs is slightly higher than that of the observed GRBs, the distribution range of the mock GRBs in the $z\text{-}log L_{\text{p,iso}}$ plane closely matches that of the observed GRBs. The median values and mean square errors of the optimal probability distribution for $\log \Gamma_c$, $\log B'$, $\log t_{\text{off}}$, and $\log R_0$ are summarized in Table 2.

6. OBSERVABLES IN THE SOFT X-RAY ENERGY BAND

With the plausible probability distribution of the physical parameters constrained from the on-axis LGRBs in Section

Table 2. Parameters of the optimal probability distributions for physical variables of the jet.

	$\log \Gamma_c$	$\log(B'/G)$	$\log(R_0/\text{cm})$	$\log(t_{\text{off}}/\text{s})$
μ	2.0	1.8	15	1.7
σ	0.1	0.2	0.3	0.48

5, we conduct Monte Carlo simulations to investigate the observables in the soft X-ray band (0.5-4 keV) for EP LGRBs, including the T_{90} duration, energy fluence, and low-energy spectral index. EP LGRBs are defined as both on-axis and off-axis LGRBs whose radiation fluxes exceed the detection threshold of WXT ($\sim 2 \times 10^{-9} \text{ erg cm}^{-2} \text{ s}^{-1}$ for a 10-s exposure; Huang et al. 2024). Furthermore, we explore the dependence of observables on different jet structures, while the structure parameters k_L and k_T are assumed to be in a range of [2, 4].

In order to generate both on-axis and off-axis bursts, we assume that the observer's line of sight is uniformly distributed over a solid angle of 4π steradians, which can be expressed as

$$\frac{dP}{\sin \theta_v d\theta_v d\phi} = \frac{1}{4\pi}. \quad (14)$$

However, when the viewing angle is too large, detecting the burst becomes challenging. For a uniform jet with sharp edges, the ratio of off-axis to on-axis $E_{\gamma,\text{iso}}$ is given by (Granot et al. 2017)

$$\frac{E_{\gamma,\text{iso}}(\theta_v)}{E_{\gamma,\text{iso}}(0)} \approx \frac{(\Gamma \theta_c)^2}{(\Gamma \theta_v)^6}, \quad \theta_v > 2\theta_c. \quad (15)$$

It is seen that a bright burst with $E_{\gamma,\text{iso}}(0) \approx 10^{54} \text{ erg}$, its equivalent energy to an off-axis viewer would abruptly decrease, e.g., $E_{\gamma,\text{iso}}(5\theta_c)$ becomes less than 10^{48} erg with typical values of Γ (~ 100) and $\theta_c \simeq$ several degrees, which is approaching the detection threshold of detectors. Thus, in order to improve the simulation efficiency, we restrict our calculation within the range of θ_v to $[0, 10\theta_c]$.

Based on the assumptions outlined above, we conduct simulations of mock EP GRBs. The probability distribution of observables for mock EP GRBs are discussed in Subsection 6.1-6.3. Our simulations reveal that off-axis events constitute a significant fraction of the EP GRB population, and more details could be found in Subsection 6.4. This finding strongly suggests that off-axis LGRBs are likely the predominant source of the enigmatic long-duration bursts observed by EP.

6.1. Duration and energy fluence

The probability distribution of T_{90} duration in the soft X-ray band for mock EP GRBs is illustrated in Figure 7. The distributions of mock on-axis GRBs and observed EP GRBs are also incorporated for comparison. For on-axis bursts, as shock-accelerated electrons cool down, the characteristic frequency of their synchrotron radiation will cross the hard X-ray band and then the lower energy bands. The hard X-ray

emission reaches peak flux before the soft X-ray emission and attenuates sooner. This results in a longer average T_{90} duration in the soft X-ray energy band compared to the hard X-ray band. As a result, the average T_{90} duration of on-axis GRBs falls within the ranges of $\sim[180 \text{ s}, 190 \text{ s}]$, for different power indices associated with the jet structures, as illustrated in Table 3. Its average T_{90} duration is lower than that ($\sim 280 \text{ s}$) of GRBs observed by EP.

For off-axis bursts, the observed burst duration Δt_{obs} related to the comoving frame duration $\Delta t'$ can be expressed by

$$\Delta t_{\text{obs}} \approx (1+z)\Gamma(1-\beta \cos \theta)\Delta t', \quad (16)$$

where θ is the angle between the observer's line of sight and the bulk velocity vectors of the uniform jet with a negligible half-opening angle. However, in realistic scenarios where the jet has a finite half-opening angle θ_c , the angle θ in Equation (16) must be replaced by a weighted average angle. This angle accounts for contributions from all jet elements within the opening angle and is defined by

$$\bar{\theta} = \frac{\int_0^{2\pi} \int_0^{\theta_c} \arccos(\sin \theta_v \sin \theta \cos \varphi + \cos \theta_v \cos \theta) \sin \theta d\theta d\varphi}{\int_0^{\theta_c} \sin \theta d\theta \int_0^{2\pi} d\varphi}, \quad (17)$$

where φ denotes the azimuthal angle of the jet element, measured relative to the jet central axis. Assuming a typical angle of $\theta_c = 2.5^\circ$, we calculate the Doppler-weighted average angles for different observational scenarios. For the on-axis case ($\theta_v = 0^\circ$), we find $\bar{\theta}_{\text{on}} \approx 1.6^\circ$, while the off-axis case ($\theta_v = 5^\circ$) yields $\bar{\theta}_{\text{off}} \approx 5.2^\circ$. Using Equation (16) with a typical Lorentz factor of $\Gamma \approx 100$, the ratio of observed durations becomes

$$\frac{t_{\text{obs}}(\bar{\theta}_{\text{off}})}{t_{\text{obs}}(\bar{\theta}_{\text{on}})} = \frac{1-\beta \cos \bar{\theta}_{\text{off}}}{1-\beta \cos \bar{\theta}_{\text{on}}} \approx 8. \quad (18)$$

As illustrated in Figure 7, the average T_{90} duration for mock EP bursts is found to lie within the ranges of $\sim[250 \text{ s}, 310 \text{ s}]$, which has a good match with that of observed EP GRBs. Note that the hard X-ray photons observed by the on-axis observer will appear as soft X-ray photons to the off-axis observer, due to the Doppler effect. The duration ratio of off-axis bursts to *Swift* bursts falls within the range of $\sim[6, 8]$, which is close to the estimate provided by the analytical equation.

The possibility distribution function of $\log F$ for on-axis bursts and EP bursts is presented in Figure 8. Owing to the beaming effect, only a small portion of photons can be detected by an off-axis observer, resulting in a lower median

energy fluence ($\sim 10^{-9} \text{ erg} \cdot \text{cm}^{-2}$) for mock EP LGRBs compared to mock on-axis LGRBs. Changes in the structure parameters of GRB jets have slight influence on the average energy fluence of EP LGRBs.

6.2. Low-energy spectral index

The probability distribution of the low-energy spectral index α of mock EP GRBs is presented in Figure 9. The distributions for mock on-axis bursts are also shown as a comparison. For on-axis bursts, the α values are primarily distributed around -0.5 , which is expected in the fast-cooling regime of the synchrotron scenario. In our model, the surrounding magnetic field of the jet decreases, and the fast-cooling electrons can have a harder energy spectrum, resulting in α values greater than -0.5 (Uhm & Zhang 2014; Geng et al. 2018a).

For mock EP LGRBs, the average value of α is approximately -0.6 , which exhibits a systematic softening compared to mock on-axis LGRBs. This discrepancy can be explained through Doppler effects. For an off-axis observer, the increased weighted average angle compared to the on-axis configuration leads to a lower Doppler factor of $\mathcal{D} \approx 1/[\Gamma(1 - \beta \cos \bar{\theta})]$. Then the observed soft X-ray emission (of $h\nu_{\text{obs}}$) corresponds to the higher comoving energy radiation (of $(1 + z)h\nu_{\text{obs}}/\mathcal{D}$), which has a softer energy spectral index. Consequently, off-axis observers will measure a systematically softer α compared to on-axis counterparts.

Notably, the distribution of the low-energy spectral index of mock GRBs may differ from that of actually observed events. The statistics of α are in contention with a synchrotron origin for GRBs (Preece et al. 1998). This contention was eased by detailed treatment of the cooling processes of electrons (Derishev et al. 2001; Daigne et al. 2011; Uhm & Zhang 2014; Zhao et al. 2014; Geng et al. 2018b), such as taking into account the synchrotron self-Compton (SSC) cooling and the decreasing of the jet magnetic field. However, the SSC cooling process is ignored in this paper in order to reduce the consumption of computing resources. The careful treatment of the cooling processes should be performed in future investigations.

6.3. The Amati and Yonetoku relations for off-axis LGRBs

The mock distribution of EP LGRBs in the $L_{\text{p,iso}}-E_{\text{p,z}}$ and $E_{\gamma,\text{iso}}-E_{\text{p,z}}$ planes is shown in Figure 10. This figure indicates that most EP LGRBs should be low-luminosity GRBs, with $E_{\gamma,\text{iso}}$ values below 10^{48} erg . Only a small fraction of them fall within the $10^{49}-10^{55} \text{ erg}$ range due to the beaming effect. Xu et al. (2023) provide a simple analytical derivation of the Amati and Yonetoku relations for both on-axis and off-axis GRBs. Their findings show that these relations depend on the value of $\theta_v - \theta_c$ when the jet is viewed off-axis. They also suggest that the slopes of both the Amati and Yonetoku relations for off-axis GRBs are lower than those for on-axis

GRBs, and a similar result can be observed in the upper left and upper right panels in Figure 10. For EP bursts, the best-fit Amati relation is $E_{\text{p}} \propto E_{\gamma,\text{iso}}^{0.298}$, and the best-fit Yonetoku relation is $E_{\text{p}} \propto L_{\text{p,iso}}^{0.275}$, with the indices k_L and k_T fixed at 2. For various power indices associated with the jet structure, the optimal slopes of the Amati and Yonetoku relations are found to lie within the ranges of $\sim[0.22, 0.31]$ and $\sim[0.21, 0.28]$, respectively. On the other hand, two EP bursts, including EP241025a and EP241030a, have been plotted in the upper left panel of Figure 10. More bursts are required to determine the slope of Amati relation for observed EP GRBs.

6.4. The detection rate of EP GRBs

We now estimate detection rate of LGRBs for EP, especially for off-axis LGRBs. The average number of LGRBs detected by *Swift* each year is approximately 70 (Lan et al. 2021). Assuming that LGRBs observed by *Swift* are primarily on-axis bursts, approximately 700 on-axis LGRBs and nearly 7,000 off-axis LGRBs are expected to occur across the celestial sphere each year. If the detection sensitivity limit is not taken into account, the detector with a field of view of $3,600 \text{ deg}^2$, similar to that of EP, will catch nearly 500 off-axis bursts and 50 on-axis bursts a year. In practice, however, only about 60% of off-axis bursts exceed the EP detection threshold, while the majority of on-axis bursts do. Consequently, EP is expected to detect ~ 370 LGRBs per year, with $\sim 90\%$ of these being off-axis events, as illustrated in Figure 11.

We also examine the number of off-axis LGRBs detected by EP that have gamma-ray counterparts. Monte Carlo simulations indicate a $\sim 10\%$ probability that an off-axis burst observed by EP would also be detectable by *Fermi* with a 5σ detection threshold of $\sim 0.5 \text{ ph cm}^{-2} \text{ s}^{-1}$, and approximately 30 off-axis bursts per year are expected to be jointly detected by both EP and *Fermi*.

Several factors may account for deviations between the simulated and observed detection rates. First, an ideal operational mode are assumed for the sky survey conducted by both EP and *Fermi*. However, in reality, the sky survey is occasionally interrupted by observations for targets of opportunity, causing some GRBs to be missed by EP or *Fermi*. These additional scientific objectives may occupy a significant portion of EP's observation time. Second, the two satellites follow different orbits and do not always observe the same regions of the sky. Consequently, a considerable fraction of bursts detected by EP may not be observed by *Fermi*. Third, in the absence of the gamma-ray observation, it is hard to identify an X-ray transient as a GRB. Many off-axis bursts detected by EP could be misclassified as fast X-ray transients with unknown origins. Additionally, some bursts detected by *Swift* may be off-axis, but our estimation assumes that all bursts are on-axis. This factor could lead to an overestima-

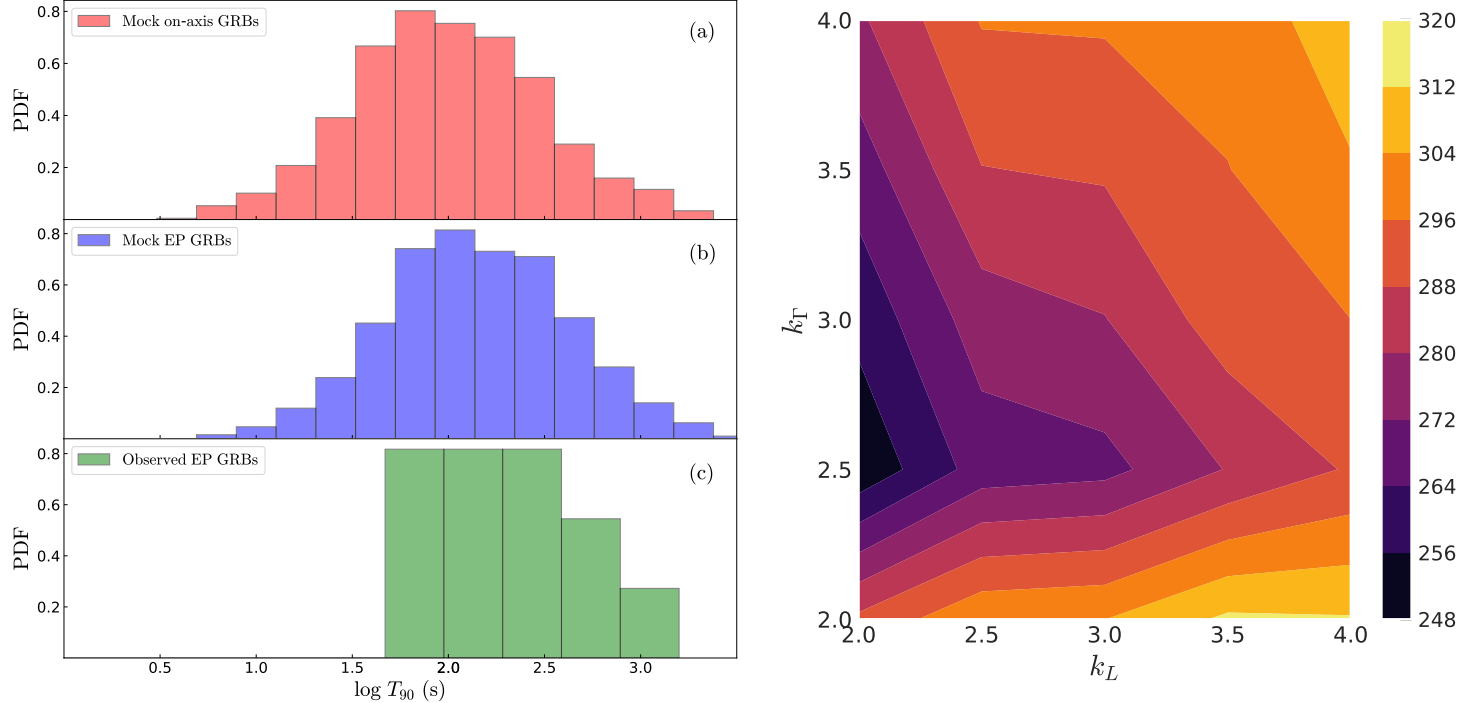


Figure 7. The T_{90} duration of EP GRBs predicted by Monte Carlo simulations in the soft X-ray band. Left panel: Panel (a) and (b) displays the probability distribution of $\log T_{90}$ duration of mock on-axis LGRBs and mock EP LGRBs, with the indices k_L and k_Γ fixed at 2. Panel (c) presents the $\log T_{90}$ duration distribution of 11 EP GRBs within the same energy band. Right panel: The dependence of the average T_{90} duration for mock LGRBs of EP on the jet structures.

Table 3. The averages of observables of EP GRBs for different jet's structures.

Bursts	On-axis GRBs				
	(k_L, k_Γ)	T_{90}/s	$\log(F/\text{erg cm}^{-2})$	α	S_A
(2, 2)	188	-5.88	-0.48	0.475	0.433
(2, 3)	185	-5.89	-0.49	0.479	0.434
(2, 4)	183	-5.89	-0.48	0.479	0.434
(3, 2)	187	-5.88	-0.48	0.478	0.434
(3, 3)	185	-5.89	-0.48	0.479	0.434
(3, 4)	184	-5.90	-0.48	0.478	0.434
(4, 2)	186	-5.89	-0.48	0.478	0.434
(4, 3)	184	-5.89	-0.48	0.478	0.434
(4, 4)	184	-5.90	-0.48	0.478	0.434

NOTE—The slopes of Amati and Yonetoku relations is denoted by S_A and S_Y .

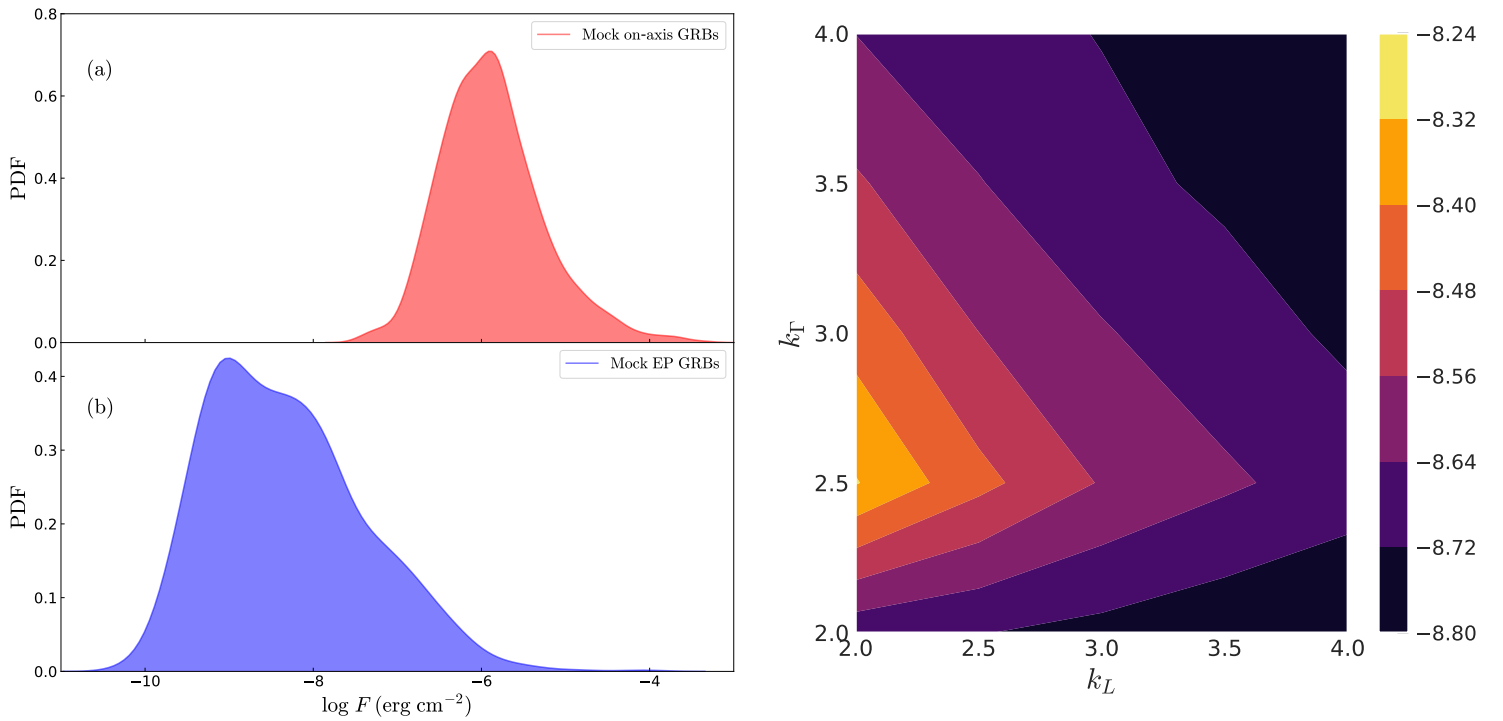


Figure 8. The energy fluence (F) of EP GRBs predicted by Monte Carlo simulations in the soft X-ray band. Left panel: Panels (a) and (b) display the probability distribution of $\log F$ of mock on-axis LGRBs and mock EP LGRBs, with the indices k_L and k_T fixed at 2. Right panel: The dependence of the average energy fluence for mock LGRBs of EP on the jet structures.

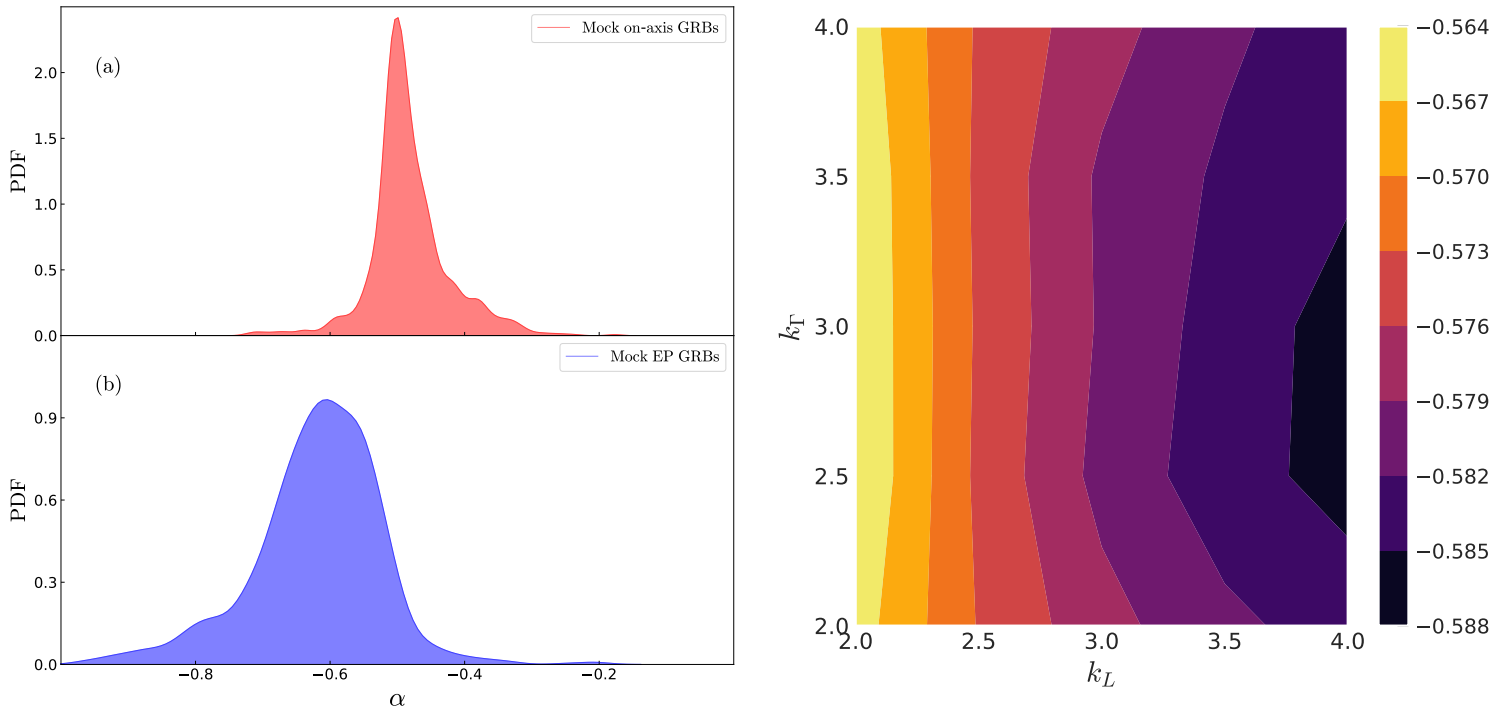


Figure 9. The low-energy spectral index α ($F_\nu \propto \nu^\alpha$) predicted by Monte Carlo simulations for EP GRBs. Left panel: Panels (a) and (b) display the probability distribution of α of mock on-axis LGRBs and mock EP LGRBs, with the indices k_L and k_T fixed at 2. Note that the mock probability distribution for LGRBs is scaled by a factor of 0.2. Right panel: The dependence of the average α for mock LGRBs of EP on the jet structures.

tion of both the off-axis and on-axis bursts across the entire sky.

Given these factors, the predicted detection rate in our simulations is expected to be higher than the actual observed rate. As mentioned in Section 2, 11 fast X-ray transients detected by EP in 2024 have been confirmed as GRBs through the detection of their gamma-ray counterparts. Our simulation results indicate that EP is expected to detect approximately 80 LGRBs per year with confirmed gamma-ray counterparts. This predicted value exceeds the current observational count, which is consistent with our initial expectations.

Currently, a fast X-ray transient detected by EP can be classified as a GRB if its gamma-ray counterpart has been observed by other satellites, such as *Fermi* and KW (Yin et al. 2024; Liu et al. 2024a). This classification approach may lead to many off-axis bursts not being identified as GRBs. Consequently, the proportion of off-axis bursts among EP-detected GRBs may be lower than 90%. As more telescopes and detectors are deployed for follow-up observations of EP-detected transients, an increasing number of these transients will be classified as GRBs through afterglow observations.

As discussed in Subsection 6.1, the average T_{90} duration in the soft-Xray band for off-axis LGRBs ranges from ap-

proximately 250 to 310 seconds, depending on the jet structure parameters, and is comparable to the average duration of GRBs detected by EP. Moreover, off-axis LGRBs constitute roughly 90% of the total LGRBs observed by EP. These findings suggest that the GRBs detected by EP may be primarily off-axis LGRBs. This conclusion can be further tested with a larger sample of GRB events detected by EP in the future, by comparing the predicted average value of various observables, such as duration, energy fluence, low-energy spectral index, and the slopes of the Amati and Yonetoku relations.

7. CONCLUSIONS AND DISCUSSION

EP has identified some GRB events, with a average duration of $\mathcal{O}(100)$ seconds, several times longer than the average duration of LGRBs observed by *Swift*. It is urgent to understand the physical origin of the intriguing EP GRBs. Based on statistical characteristics of LGRBs accumulated in the past, we constrain the parameters of GRB jets within the synchrotron emission scenario and investigate the distributions of observables in the soft X-ray band for LGRBs detected by EP, including the duration, energy fluence, and low-energy spectral index. The Amati and Yonetoku relations for EP LGRBs are also studied. Additionally, the dependence of ob-

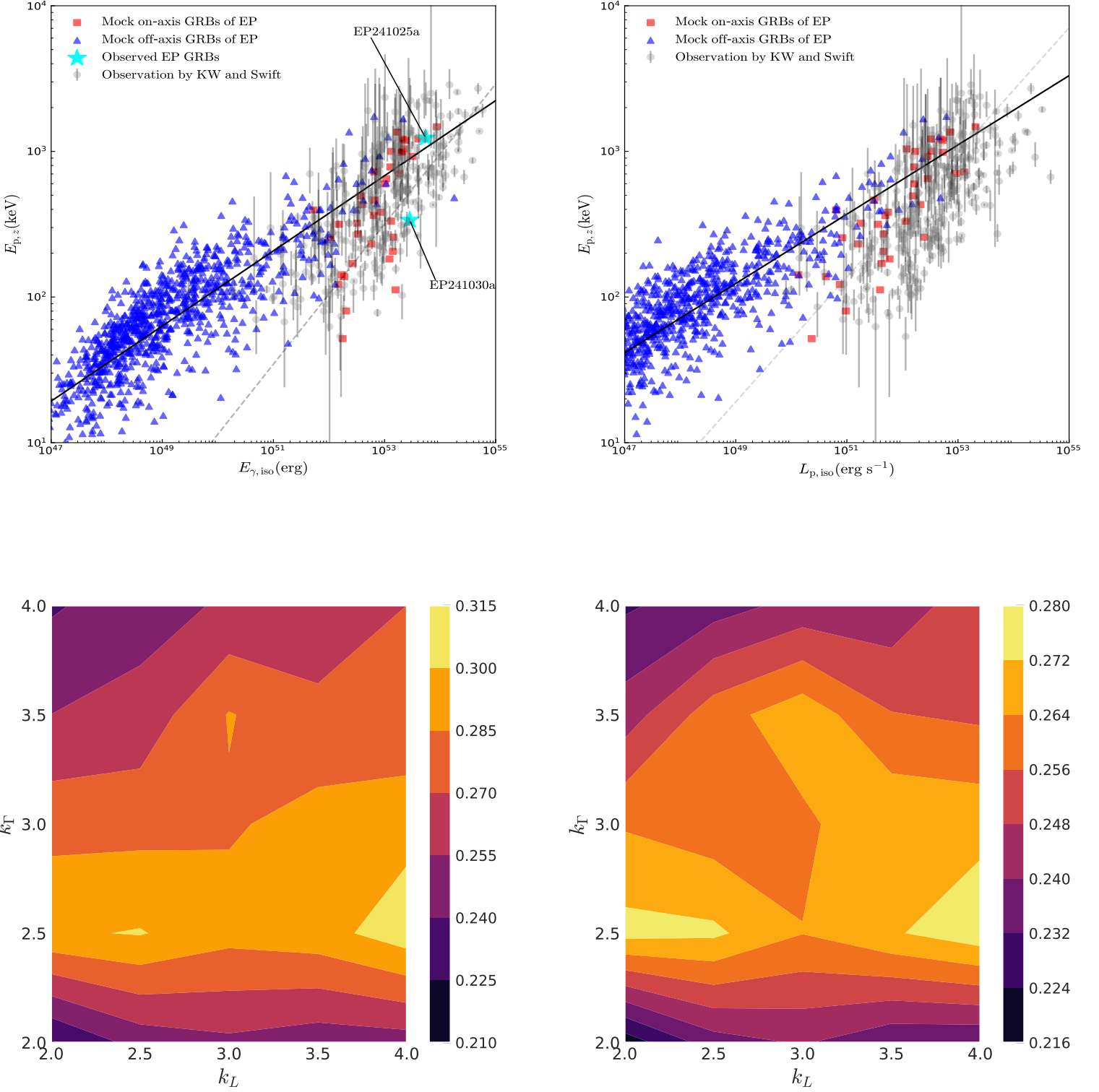


Figure 10. Slopes of the Amati and Yonetoku relations predicted by Monte Carlo simulations for EP GRBs. Upper left and right panels: The distribution of mock LGRBs of EP in the $L_{p,\text{iso}}-E_{p,z}$ and $E_{\gamma,\text{iso}}-E_{p,z}$ planes. The grey circle dots represent observed LGRBs from Tsvetkova et al. (2021), and the red and blue triangular dots show our mock results for EP LGRBs. The solid line and the dashed line correspond to the best-fit result for mock and observed samples, with the indices k_L and k_T fixed at 2. Lower left and right panels: The dependence of the slopes of the Amati (left) and Yonetoku (right) relations for EP LGRBs on the jet structures.

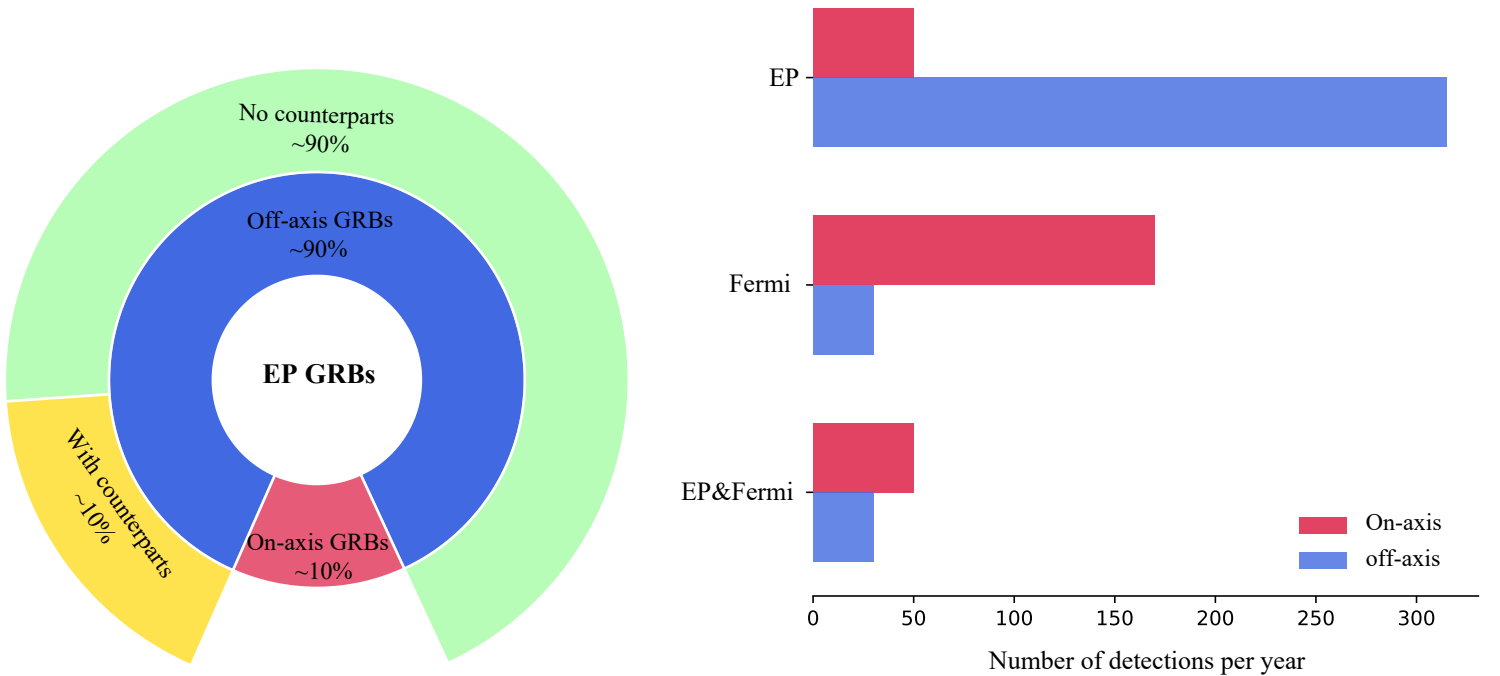


Figure 11. Left panel: The estimated distribution of different components in the LGRB sample observed by EP. The inner ring shows the proportion of the off-axis LGRBs (red) and the on-axis LGRBs (blue) among the EP GRBs. The outer ring shows the proportion of bursts with (yellow) and without (green) gamma-ray counterparts among the off-axis GRBs. Right panel: The estimated detection rates of the on-axis (red) or off-axis GRBs (blue) for EP, *Fermi*, and the joint of EP and *Fermi*.

servables on different jet structures is explored. Our simulation results suggest that the new population with particularly long durations observed by EP may primarily consist of off-axis LGRBs.

Assuming a viewing angle of within $10\theta_c$, we examine the observables in the soft X-ray band during the main burst for both on-axis and off-axis LGRBs. For on-axis LGRBs, the average T_{90} duration is approximately 180 s. A larger viewing angle results in a greater average angle between the motion direction of jet elements and the observer's line of sight. Due to the Doppler effect, off-axis LGRBs exhibit a longer T_{90} duration. As off-axis LGRBs account for $\sim 90\%$ of burst observed by EP, the average duration of EP bursts falls within the ranges of $\sim [250, 310]$ s for various power-law indices associated with the jet structure. The duration ratio of LGRBs observed by EP in the soft X-ray band to on axis LGRBs observed in the gamma-ray and hard X-ray band is ~ 7 .

Monte Carlo simulations reveal that the average energy fluence of on-axis LGRBs is about 10^{-6} erg · cm $^{-2}$. Due to the beaming effect, only a small portion of photons are detected by an off-axis observer, resulting in a lower average energy fluence of approximately 10^{-9} erg · cm $^{-2}$ for EP LGRBs. We find that the structure parameters of GRB jets have little influence on the average energy fluence of EP LGRBs.

The values of low-energy spectral index, α , for the on-axis LGRBs are primarily distributed around -0.5, which is expected in the fast-cooling regime of the synchrotron scenario. In our scenario, the surrounding magnetic field of the jet decreases, and the fast-cooling electrons can have a harder energy spectrum, with α that can be greater than -0.5. For the LGRBs detected by EP, the average value of α is approximately -0.6, and α exhibits a broad distribution range from -0.9 to 0, and is almost independent of the structure parameters of GRB jets.

The Amati and Yonetoku relations for EP LGRBs are also explored. It is seen that the EP LGRBs form a unique population in the $E_{\gamma, \text{iso}} - E_{\text{p},z}$ and $L_{\text{p}, \text{iso}} - E_{\text{p},z}$ diagrams. Due to the beaming effect, only a small fraction of EP LGRBs fall within the $10^{49} - 10^{55}$ erg range. The slopes of both the Amati and Yonetoku relations for these bursts are lower than those for on-axis LGRBs. For different structure parameters of GRB jets, the optimal slopes of Amati and Yonetoku relations are found to lie within the ranges of $\sim [0.22, 0.31]$ and $\sim [0.21, 0.28]$, respectively. As more GRB data from EP is collected, this hypothesis can be tested by directly comparing these simulated features, including the distribution of T_{90} duration and energy fluence, the slopes of the Amati and Yonetoku relations, with the observational results.

Based on the average number of LGRBs detected by *Swift* each year, the optimistic detection rate of LGRBs by EP/WXT is approximately 370 per year, among which the off-axis LGRBs account for approximately 90%. We also

estimate the number of off-axis LGRBs detected by EP that have gamma-ray counterparts, and approximately 30 off-axis bursts per year are expected to be jointly detected by both EP and *Fermi*. The idealized assumption of sky survey operations in simulations may cause deviations between the simulated and observed detection rates.

In the main text, a power-law structured jet is assumed, and it is found that various jet parameters have only a minor influence on the distribution of observables for off-axis bursts. It is expected that Monte Carlo simulations based on a Gaussian jet will yield similar results to those obtained in the power-law structured jet case.

In the literature, it has been argued that there are many orphan afterglows in the sky, which could be produced by relativistic outflows whose motion is not pointed toward us (Rhoads 1997). These outflows are essentially off-axis GRB jets. They do not show up as GRBs simply because our line of sight is not on the axis. However, their afterglow may still be observable when the outflow is significantly decelerated at late stages so that softer photons are emitted into a much wider solid angle. Such afterglows are called orphan afterglows because they are not associated with any GRBs. Observing these orphan afterglows may potentially help measure the beaming angle of normal GRBs (Mészáros et al. 1999), but no firm detection of these fascinating phenomena has been established yet despite extensive observational efforts (Ho et al. 2022). We argue that the X-ray transients detected by EP may be the early counterpart of orphan afterglows. It is thus solicited that these X-ray transients be followed and monitored by large telescopes at multi-wavelengths, which may hopefully lead to the discovery of orphan afterglows. Note that orphan afterglows may also be produced by “failed GRBs”, i.e. isotropic baryon-contaminated fireballs with the Lorentz factor much less than 100 (Huang et al. 2002). These two kinds of orphan afterglows, i.e., off-axis ones and failed-GRB-induced events, could be discriminated by examining their decaying behaviors at late stages (Huang et al. 2002).

Extragalactic fast X-ray transients (FXTs), short-duration (\sim ks) X-ray flashes of unknown origin, may also be linked to orphan afterglows. Wichern et al. (2024) have explored the possible connection between FXTs and the afterglows of off-axis, merger-induced GRBs. Their analysis suggests that a slightly off-axis viewing angle of $\theta_{\text{obs}} \approx (2.2 - 3)\theta_c$ and a structured jet are necessary to explain the shallow temporal indices ($|\alpha| \leq 0.3$) observed in FXT light curves, which can not be accounted for a uniform jet at any viewing angle. Future observations of FXTs by EP will help clarify the potential connection between GRBs and FXTs and may eventually identify the progenitors of some FXTs.

The long duration in the soft X-ray band may also hint at the intrinsic characteristics of some LGRBs themselves. Ex-

cept for ultra-relativistic jets launched from the GRB central engine sufficiently discussed in the literature, there is growing evidence that the mildly relativistic jets (Sun et al. 2024b) or weak jets (Sun et al. 2024a) could play significant roles. Radiation from these jets may be concentrated in the soft X-ray band and obscured by emissions from strong jets, making it difficult to identify them in the prompt and afterglow phase. The fraction of these intrinsic long GRBs in EP GRBs remains highly uncertain and invokes further studies.

The successful launch of EP in early 2024 opened up a new window into the transient X-ray sky. EP is expected to yield a substantial amount of observational data in the near future, including soft X-ray emissions during the main burst of GRBs, X-ray-rich GRBs that gamma-ray detectors may miss, and high-redshift GRBs. This will help us to unveil the physical origins of GRBs and shed light on the mysteries of the early universe.

We thank the anonymous referee for constructive suggestions. We also appreciate Bing Zhang for his valuable input and Chen-Ran Hu for the helpful discussions. This work is based on data obtained with Einstein Probe, a space mission supported by Strategic Priority Program on Space Science of Chinese Academy of Sciences, in collaboration with ESA, MPE and CNES (Grant No. XDA15310000). This study is partially supported by the National Natural Science Foundation of China (grant Nos. 12273113, 12321003, 12233002, 12393812, 12393813), the National SKA Program of China (grant Nos. 2022SKA0130100, 2020SKA0120300, 2020SKA0120302), the International Partnership Program of Chinese Academy of Sciences for Grand Challenges (114332KYSB20210018), the National Key R&D Program of China (2021YFA0718500), the Strategic Priority Research Program of the Chinese Academy of Sciences (grant No. XDB0550400). Jin-Jun Geng acknowledges support from the Youth Innovation Promotion Association (2023331). Hao-Xuan Gao acknowledges support from Jiangsu Funding Program for Excellent Postdoctoral Talent. Yong-Feng Huang also acknowledges the support from the Xinjiang Tianchi Program.

REFERENCES

Aloy, M. A., Janka, H. T., & Müller, E. 2005, A&A, 436, 273, doi: [10.1051/0004-6361:20041865](https://doi.org/10.1051/0004-6361:20041865)

Amati, L. 2006, MNRAS, 372, 233, doi: [10.1111/j.1365-2966.2006.10840.x](https://doi.org/10.1111/j.1365-2966.2006.10840.x)

Amati, L., Frontera, F., Tavani, M., et al. 2002, A&A, 390, 81, doi: [10.1051/0004-6361:20020722](https://doi.org/10.1051/0004-6361:20020722)

Band, D., Matteson, J., Ford, L., et al. 1993, ApJ, 413, 281, doi: [10.1086/172995](https://doi.org/10.1086/172995)

Band, D. L. 1997, The Astrophysical Journal, 486, 928, doi: [10.1086/304566](https://doi.org/10.1086/304566)

Beloborodov, A. M. 2010, MNRAS, 407, 1033, doi: [10.1111/j.1365-2966.2010.16770.x](https://doi.org/10.1111/j.1365-2966.2010.16770.x)

Berger, E. 2014, ARA&A, 52, 43, doi: [10.1146/annurev-astro-081913-035926](https://doi.org/10.1146/annurev-astro-081913-035926)

Bernardini, M. G., Campana, S., Ghisellini, G., et al. 2013, ApJ, 775, 67, doi: [10.1088/0004-637X/775/1/67](https://doi.org/10.1088/0004-637X/775/1/67)

Blandford, R. D., & Znajek, R. L. 1977, MNRAS, 179, 433, doi: [10.1093/mnras/179.3.433](https://doi.org/10.1093/mnras/179.3.433)

Bloom, J. S., Frail, D. A., & Sari, R. 2001, The Astronomical Journal, 121, 2879, doi: [10.1086/321093](https://doi.org/10.1086/321093)

Bromberg, O., Nakar, E., Piran, T., & Sari, R. 2011, ApJ, 740, 100, doi: [10.1088/0004-637X/740/2/100](https://doi.org/10.1088/0004-637X/740/2/100)

Burgess, J. M., Bégué, D., Greiner, J., et al. 2020, Nature Astronomy, 4, 174, doi: [10.1038/s41550-019-0911-z](https://doi.org/10.1038/s41550-019-0911-z)

Burlon, D., Ghirlanda, G., Ghisellini, G., et al. 2008, ApJL, 685, L19, doi: [10.1086/592350](https://doi.org/10.1086/592350)

Cheng, H. Q., Wang, W. X., Yuan, W., et al. 2024, GRB Coordinates Network, 36138, 1

Cheng, L. X., Ma, Y. Q., Cheng, K. S., Lu, T., & Zhou, Y. Y. 1995, A&A, 300, 746

Dado, S., & Dar, A. 2012, ApJ, 749, 100, doi: [10.1088/0004-637X/749/2/100](https://doi.org/10.1088/0004-637X/749/2/100)

Dai, Z. G., & Lu, T. 2001, The Astrophysical Journal, 551, 249, doi: [10.1086/320056](https://doi.org/10.1086/320056)

Daigne, F., Bošnjak, Ž., & Dubus, G. 2011, A&A, 526, A110, doi: [10.1051/0004-6361/201015457](https://doi.org/10.1051/0004-6361/201015457)

Daigne, F., Rossi, E. M., & Mochkovitch, R. 2006, MNRAS, 372, 1034, doi: [10.1111/j.1365-2966.2006.10837.x](https://doi.org/10.1111/j.1365-2966.2006.10837.x)

Demianski, M., Piedipalumbo, E., Sawant, D., & Amati, L. 2017, A&A, 598, A112, doi: [10.1051/0004-6361/201628909](https://doi.org/10.1051/0004-6361/201628909)

Derishev, E. V., Kocharyan, V. V., & Kocharyan, V. V. 2001, A&A, 372, 1071, doi: [10.1051/0004-6361:20010586](https://doi.org/10.1051/0004-6361:20010586)

Eichler, D., & Levinson, A. 2004, ApJL, 614, L13, doi: [10.1086/425310](https://doi.org/10.1086/425310)

Eichler, D., Livio, M., Piran, T., & Schramm, D. N. 1989, Nature, 340, 126, doi: [10.1038/340126a0](https://doi.org/10.1038/340126a0)

Firmani, C., Avila-Reese, V., Ghisellini, G., & Tutukov, A. V. 2004, ApJ, 611, 1033, doi: [10.1086/422186](https://doi.org/10.1086/422186)

Fu, Y. C., Jiang, S. Q., Hu, J. W., et al. 2024, GRB Coordinates Network, 37088, 1

Gao, H.-X., Geng, J.-J., & Huang, Y.-F. 2021, *Astronomy & Astrophysics*, 656, A134, doi: [10.1051/0004-6361/202141647](https://doi.org/10.1051/0004-6361/202141647)

Gao, H.-X., Geng, J.-J., Sun, T.-R., et al. 2024, *The Astrophysical Journal*, 971, 81, doi: [10.3847/1538-4357/ad5443](https://doi.org/10.3847/1538-4357/ad5443)

Gao, H.-X., Geng, J.-J., Hu, L., et al. 2022, *MNRAS*, 516, 453, doi: [10.1093/mnras/stac2215](https://doi.org/10.1093/mnras/stac2215)

Geng, J.-J., Huang, Y.-F., Wu, X.-F., Song, L.-M., & Zong, H.-S. 2018a, *ApJ*, 862, 115, doi: [10.3847/1538-4357/aacd05](https://doi.org/10.3847/1538-4357/aacd05)

Geng, J.-J., Huang, Y.-F., Wu, X.-F., Zhang, B., & Zong, H.-S. 2018b, *ApJS*, 234, 3, doi: [10.3847/1538-4365/aa9e84](https://doi.org/10.3847/1538-4365/aa9e84)

Geng, J. J., Wu, X. F., Huang, Y. F., Li, L., & Dai, Z. G. 2016a, *ApJ*, 825, 107, doi: [10.3847/0004-637X/825/2/107](https://doi.org/10.3847/0004-637X/825/2/107)

Geng, J.-J., Zhang, B., Kölligan, A., Kuiper, R., & Huang, Y.-F. 2019, *ApJL*, 877, L40, doi: [10.3847/2041-8213/ab224b](https://doi.org/10.3847/2041-8213/ab224b)

Geng, J.-J., Zhang, B., & Kuiper, R. 2016b, *ApJ*, 833, 116, doi: [10.3847/1538-4357/833/1/116](https://doi.org/10.3847/1538-4357/833/1/116)

Granot, J., Guetta, D., & Gill, R. 2017, *ApJL*, 850, L24, doi: [10.3847/2041-8213/aa991d](https://doi.org/10.3847/2041-8213/aa991d)

Granot, J., Panaiteescu, A., Kumar, P., & Woosley, S. E. 2002, *ApJL*, 570, L61, doi: [10.1086/340991](https://doi.org/10.1086/340991)

Guetta, D., & Della Valle, M. 2007, *ApJL*, 657, L73, doi: [10.1086/511417](https://doi.org/10.1086/511417)

Haggard, D., Nynka, M., Ruan, J. J., et al. 2017, *ApJL*, 848, L25, doi: [10.3847/2041-8213/aa8ede](https://doi.org/10.3847/2041-8213/aa8ede)

Ho, A. Y., Perley, D. A., Yao, Y., et al. 2022, *The Astrophysical Journal*, 938, 85, doi: [10.3847/1538-4357/ac8bd0](https://doi.org/10.3847/1538-4357/ac8bd0)

Horváth, I., & Tóth, B. G. 2016, *Ap&SS*, 361, 155, doi: [10.1007/s10509-016-2748-6](https://doi.org/10.1007/s10509-016-2748-6)

Hu, D. F., Zheng, T. C., Wang, B. T., et al. 2024a, GRB Coordinates Network, 38335, 1

Hu, J. W., Huang, M. Q., Liu, Z. Y., et al. 2024b, GRB Coordinates Network, 38239, 1

Hu, J. W., Wang, Y., He, H., et al. 2024c, GRB Coordinates Network, 37834, 1

Hu, J. W., Zhao, D. H., Liu, Y., et al. 2024d, GRB Coordinates Network, 36053, 1

Hu, Y.-D., Liang, E.-W., Xi, S.-Q., et al. 2014, *ApJ*, 789, 145, doi: [10.1088/0004-637X/789/2/145](https://doi.org/10.1088/0004-637X/789/2/145)

Huang, Y., Zhang, J., Tao, L., et al. 2024, *Experimental Astronomy*, 57, 3, doi: [10.1007/s10686-024-09924-0](https://doi.org/10.1007/s10686-024-09924-0)

Huang, Y. F., Dai, Z. G., & Lu, T. 2002, *MNRAS*, 332, 735, doi: [10.1046/j.1365-8711.2002.05334.x](https://doi.org/10.1046/j.1365-8711.2002.05334.x)

Huang, Y. F., Gou, L. J., Dai, Z. G., & Lu, T. 2000, *ApJ*, 543, 90, doi: [10.1086/317076](https://doi.org/10.1086/317076)

Ioka, K., & Nakamura, T. 2018, *Progress of Theoretical and Experimental Physics*, 2018, 043E02, doi: [10.1093/ptep/pty036](https://doi.org/10.1093/ptep/pty036)

Izzo, L., Kuhn, O., Rossi, A., et al. 2024, GRB Coordinates Network, 37925, 1

Kaneko, Y., Preece, R. D., Briggs, M. S., et al. 2006, *ApJS*, 166, 298, doi: [10.1086/505911](https://doi.org/10.1086/505911)

Kathirgamaraju, A., Barniol Duran, R., & Giannios, D. 2018, *MNRAS*, 473, L121, doi: [10.1093/mnrasl/slx175](https://doi.org/10.1093/mnrasl/slx175)

Kocevski, D. 2012, *ApJ*, 747, 146, doi: [10.1088/0004-637X/747/2/146](https://doi.org/10.1088/0004-637X/747/2/146)

Koshut, T. M., Kouveliotou, C., Paciesas, W. S., et al. 1995, *ApJ*, 452, 145, doi: [10.1086/176286](https://doi.org/10.1086/176286)

Kouveliotou, C., Meegan, C. A., Fishman, G. J., et al. 1993, *ApJL*, 413, L101, doi: [10.1086/186969](https://doi.org/10.1086/186969)

Kumar, P., & Granot, J. 2003, *ApJ*, 591, 1075, doi: [10.1086/375186](https://doi.org/10.1086/375186)

Kumar, P., & Zhang, B. 2015, *PhR*, 561, 1, doi: [10.1016/j.physrep.2014.09.008](https://doi.org/10.1016/j.physrep.2014.09.008)

Lamb, G. P., & Kobayashi, S. 2017, *MNRAS*, 472, 4953, doi: [10.1093/mnras/stx2345](https://doi.org/10.1093/mnras/stx2345)

Lan, G.-X., Wei, J.-J., Zeng, H.-D., Li, Y., & Wu, X.-F. 2021, *MNRAS*, 508, 52, doi: [10.1093/mnras/stab2508](https://doi.org/10.1093/mnras/stab2508)

Lan, L., Lü, H.-J., Zhong, S.-Q., et al. 2018, *ApJ*, 862, 155, doi: [10.3847/1538-4357/aacd6](https://doi.org/10.3847/1538-4357/aacd6)

Lazzati, D. 2005, *MNRAS*, 357, 722, doi: [10.1111/j.1365-2966.2005.08687.x](https://doi.org/10.1111/j.1365-2966.2005.08687.x)

Lazzati, D., Perna, R., Morsony, B. J., et al. 2018, *PhRvL*, 120, 241103, doi: [10.1103/PhysRevLett.120.241103](https://doi.org/10.1103/PhysRevLett.120.241103)

Levinson, A., & Eichler, D. 2003, *ApJL*, 594, L19, doi: [10.1086/378487](https://doi.org/10.1086/378487)

Li, D. Y., Liu, Z. Y., Huang, M. Q., et al. 2024a, GRB Coordinates Network, 37864, 1

Li, D. Y., Xu, X. P., Wang, B. T., et al. 2024b, GRB Coordinates Network, 37492, 1

Li, L.-B., Geng, J.-J., Huang, Y.-F., & Li, B. 2019, *ApJ*, 880, 39, doi: [10.3847/1538-4357/ab275d](https://doi.org/10.3847/1538-4357/ab275d)

Li, R. Z., Lin, H., Li, S. S., et al. 2024c, GRB Coordinates Network, 38027, 1

Lian, T. Y., Pan, X., Ling, Z. X., et al. 2024a, GRB Coordinates Network, 36091, 1

—. 2024b, GRB Coordinates Network, 36086, 1

Liang, E., Zhang, B., Virgili, F., & Dai, Z. G. 2007, *ApJ*, 662, 1111, doi: [10.1086/517959](https://doi.org/10.1086/517959)

Liang, E. W., Zhang, B., O'Brien, P. T., et al. 2006, *ApJ*, 646, 351, doi: [10.1086/504684](https://doi.org/10.1086/504684)

Liang, Y. F., Liu, H. Y., Mao, X., et al. 2024, GRB Coordinates Network, 37214, 1

Lipunov, V. M., Postnov, K. A., & Prokhorov, M. E. 2001, *Astronomy Reports*, 45, 236, doi: [10.1134/1.1353364](https://doi.org/10.1134/1.1353364)

Liu, Y., Sun, H., Xu, D., et al. 2024a, arXiv e-prints, arXiv:2404.16425, doi: [10.48550/arXiv.2404.16425](https://doi.org/10.48550/arXiv.2404.16425)

Liu, Z. Y., Huang, M. Q., Dai, C. Y., et al. 2024b, GRB Coordinates Network, 38214, 1

Lu, R.-J., Wei, J.-J., Liang, E.-W., et al. 2012, *ApJ*, 756, 112, doi: [10.1088/0004-637X/756/2/112](https://doi.org/10.1088/0004-637X/756/2/112)

Meegan, C. A., Fishman, G. J., Wilson, R. B., et al. 1992, *Nature*, 355, 143, doi: [10.1038/355143a0](https://doi.org/10.1038/355143a0)

Meng, Y.-Z., Geng, J.-J., Zhang, B.-B., et al. 2018, *ApJ*, 860, 72, doi: [10.3847/1538-4357/aac2d9](https://doi.org/10.3847/1538-4357/aac2d9)

Mészáros, P., Rees, M., & Wijers, R. 1999, *New Astronomy*, 4, 303

Mészáros, P., & Rees, M. J. 2000, *ApJ*, 530, 292, doi: [10.1086/308371](https://doi.org/10.1086/308371)

Mészáros, P., Rees, M. J., & Papathanassiou, H. 1994, *ApJ*, 432, 181, doi: [10.1086/174559](https://doi.org/10.1086/174559)

Mészáros, P., Rees, M. J., & Wijers, R. A. M. J. 1998, *ApJ*, 499, 301, doi: [10.1086/305635](https://doi.org/10.1086/305635)

Minaev, P. Y., & Pozanenko, A. S. 2020, *MNRAS*, 492, 1919, doi: [10.1093/mnras/stz3611](https://doi.org/10.1093/mnras/stz3611)

Mochkovitch, R., & Nava, L. 2015, *A&A*, 577, A31, doi: [10.1051/0004-6361/201424490](https://doi.org/10.1051/0004-6361/201424490)

Morsony, B. J., Lazzati, D., & Begelman, M. C. 2010, *ApJ*, 723, 267, doi: [10.1088/0004-637X/723/1/267](https://doi.org/10.1088/0004-637X/723/1/267)

Nagakura, H., Hotokezaka, K., Sekiguchi, Y., Shibata, M., & Ioka, K. 2014, *ApJL*, 784, L28, doi: [10.1088/2041-8205/784/2/L28](https://doi.org/10.1088/2041-8205/784/2/L28)

Nakar, E., & Piran, T. 2016, *The Astrophysical Journal*, 834, 28, doi: [10.3847/1538-4357/834/1/28](https://doi.org/10.3847/1538-4357/834/1/28)

Nava, L., Salvaterra, R., Ghirlanda, G., et al. 2012, *MNRAS*, 421, 1256, doi: [10.1111/j.1365-2966.2011.20394.x](https://doi.org/10.1111/j.1365-2966.2011.20394.x)

Norris, J. P., Marani, G. F., & Bonnell, J. T. 2000, *ApJ*, 534, 248, doi: [10.1086/308725](https://doi.org/10.1086/308725)

Norris, J. P., Nemiroff, R. J., Bonnell, J. T., et al. 1996, *ApJ*, 459, 393, doi: [10.1086/176902](https://doi.org/10.1086/176902)

O'Connor, B., Beniamini, P., & Gill, R. 2024, *MNRAS*, 533, 1629, doi: [10.1093/mnras/stae1941](https://doi.org/10.1093/mnras/stae1941)

Paciesas, W. S., & Fermi GBM Collaboration. 2012, in *American Astronomical Society Meeting Abstracts*, Vol. 219, American Astronomical Society Meeting Abstracts #219, 149.12

Paczynski, B., & Xu, G. 1994, *ApJ*, 427, 708, doi: [10.1086/174178](https://doi.org/10.1086/174178)

Pan, X., Zhao, D. H., Peng, J. Q., et al. 2024, *GRB Coordinates Network*, 36330, 1

Pe'er, A., Mészáros, P., & Rees, M. J. 2006, *ApJ*, 642, 995, doi: [10.1086/501424](https://doi.org/10.1086/501424)

Peng, J. Q., Shui, Q. C., Dai, C. Y., et al. 2024, *GRB Coordinates Network*, 36810, 1

Pescalli, A., Ghirlanda, G., Salafia, O. S., et al. 2015, *MNRAS*, 447, 1911, doi: [10.1093/mnras/stu2482](https://doi.org/10.1093/mnras/stu2482)

Petrosian, V., Kitanidis, E., & Kocevski, D. 2015, *ApJ*, 806, 44, doi: [10.1088/0004-637X/806/1/44](https://doi.org/10.1088/0004-637X/806/1/44)

Piran, T. 2004, *Reviews of Modern Physics*, 76, 1143, doi: [10.1103/RevModPhys.76.1143](https://doi.org/10.1103/RevModPhys.76.1143)

Preece, R. D., Briggs, M. S., Mallozzi, R. S., et al. 1998, *ApJL*, 506, L23, doi: [10.1086/311644](https://doi.org/10.1086/311644)

—. 2000, *ApJS*, 126, 19, doi: [10.1086/313289](https://doi.org/10.1086/313289)

Qin, Y.-P., & Chen, Z.-F. 2013, *MNRAS*, 430, 163, doi: [10.1093/mnras/sts547](https://doi.org/10.1093/mnras/sts547)

Ramirez-Ruiz, E., Granot, J., Kouveliotou, C., et al. 2005, *ApJL*, 625, L91, doi: [10.1086/431237](https://doi.org/10.1086/431237)

Rees, M. J., & Mészáros, P. 1994, *ApJL*, 430, L93, doi: [10.1086/187446](https://doi.org/10.1086/187446)

—. 2005, *ApJ*, 628, 847, doi: [10.1086/430818](https://doi.org/10.1086/430818)

Rhoads, J. E. 1997, *ApJL*, 487, L1, doi: [10.1086/310876](https://doi.org/10.1086/310876)

Ridnaia, A., Frederiks, D., Lysenko, A., et al. 2024, *GRB Coordinates Network*, 37982, 1

Rossi, E., Lazzati, D., & Rees, M. J. 2002, *MNRAS*, 332, 945, doi: [10.1046/j.1365-8711.2002.05363.x](https://doi.org/10.1046/j.1365-8711.2002.05363.x)

Ryan, G., van Eerten, H., Piro, L., & Troja, E. 2020, *ApJ*, 896, 166, doi: [10.3847/1538-4357/ab93cf](https://doi.org/10.3847/1538-4357/ab93cf)

Rybicki, G. B., & Lightman, A. P. 1979, *Radiative processes in astrophysics*

Ryde, F., Pe'er, A., Nymark, T., et al. 2011, *MNRAS*, 415, 3693, doi: [10.1111/j.1365-2966.2011.18985.x](https://doi.org/10.1111/j.1365-2966.2011.18985.x)

Sakamoto, T., Barthelmy, S. D., Barbier, L., et al. 2008, *ApJS*, 175, 179, doi: [10.1086/523646](https://doi.org/10.1086/523646)

Sakamoto, T., Barthelmy, S. D., Baumgartner, W. H., et al. 2011, *ApJS*, 195, 2, doi: [10.1088/0067-0049/195/1/2](https://doi.org/10.1088/0067-0049/195/1/2)

Salvaterra, R., & Chincarini, G. 2007, *ApJL*, 656, L49, doi: [10.1086/512606](https://doi.org/10.1086/512606)

Salvaterra, R., Della Valle, M., Campana, S., et al. 2009, *Nature*, 461, 1258, doi: [10.1038/nature08445](https://doi.org/10.1038/nature08445)

Salvaterra, R., Campana, S., Vergani, S. D., et al. 2012, *ApJ*, 749, 68, doi: [10.1088/0004-637X/749/1/68](https://doi.org/10.1088/0004-637X/749/1/68)

Spruit, H. C., Daigne, F., & Drenkhahn, G. 2001, *A&A*, 369, 694, doi: [10.1051/0004-6361:20010131](https://doi.org/10.1051/0004-6361:20010131)

Sun, H., Li, W. X., Liu, L. D., et al. 2024a, *arXiv e-prints*, arXiv:2410.02315, doi: [10.48550/arXiv.2410.02315](https://doi.org/10.48550/arXiv.2410.02315)

Sun, T.-R., Geng, J.-J., Yan, J.-Z., et al. 2024b, *ApJL* in press, arXiv:2409.17983, doi: [10.48550/arXiv.2409.17983](https://doi.org/10.48550/arXiv.2409.17983)

Svinkin, D., Frederiks, D., Lysenko, A., et al. 2024, *GRB Coordinates Network*, 37927, 1

Tavani, M. 1996, *ApJ*, 466, 768, doi: [10.1086/177551](https://doi.org/10.1086/177551)

Tian, X., Peng, H. L., Mao, X., et al. 2024, *GRB Coordinates Network*, 37648, 1

Troja, E., Piro, L., van Eerten, H., et al. 2017, *Nature*, 551, 71, doi: [10.1038/nature24290](https://doi.org/10.1038/nature24290)

Troja, E., van Eerten, H., Ryan, G., et al. 2019, *MNRAS*, 489, 1919, doi: [10.1093/mnras/stz2248](https://doi.org/10.1093/mnras/stz2248)

Tsvetkova, A., Frederiks, D., Golenetskii, S., et al. 2017, *ApJ*, 850, 161, doi: [10.3847/1538-4357/aa96af](https://doi.org/10.3847/1538-4357/aa96af)

Tsvetkova, A., Frederiks, D., Svinkin, D., et al. 2021, *ApJ*, 908, 83, doi: [10.3847/1538-4357/abd569](https://doi.org/10.3847/1538-4357/abd569)

Uhm, Z. L., & Zhang, B. 2014, *Nature Physics*, 10, 351, doi: [10.1038/nphys2932](https://doi.org/10.1038/nphys2932)

—. 2016, *ApJL*, 824, L16, doi: [10.3847/2041-8205/824/1/L16](https://doi.org/10.3847/2041-8205/824/1/L16)

Uhm, Z. L., Zhang, B., & Racusin, J. 2018, *ApJ*, 869, 100, doi: [10.3847/1538-4357/aaeb30](https://doi.org/10.3847/1538-4357/aaeb30)

van Putten, M. H. P. M., & Levinson, A. 2003, *The Astrophysical Journal*, 584, 937, doi: [10.1086/345900](https://doi.org/10.1086/345900)

Vlahakis, N., Peng, F., & Königl, A. 2003, *ApJL*, 594, L23, doi: [10.1086/378580](https://doi.org/10.1086/378580)

von Kienlin, A., Meegan, C. A., Paciesas, W. S., et al. 2020, *ApJ*, 893, 46, doi: [10.3847/1538-4357/ab7a18](https://doi.org/10.3847/1538-4357/ab7a18)

Wanderman, D., & Piran, T. 2010, *MNRAS*, 406, 1944, doi: [10.1111/j.1365-2966.2010.16787.x](https://doi.org/10.1111/j.1365-2966.2010.16787.x)

Wang, X.-G., Zhang, B., Liang, E.-W., et al. 2018, *ApJ*, 859, 160, doi: [10.3847/1538-4357/aabc13](https://doi.org/10.3847/1538-4357/aabc13)

Wang, Y., Sun, H., Wang, Y. L., et al. 2024, GRB Coordinates Network, 37034, 1

Wichern, H. C. I., Ravasio, M. E., Jonker, P. G., et al. 2024, *A&A*, 690, A101, doi: [10.1051/0004-6361/202450116](https://doi.org/10.1051/0004-6361/202450116)

Wu, B., & Fenimore, E. 2000, *ApJL*, 535, L29, doi: [10.1086/312700](https://doi.org/10.1086/312700)

Wu, Q. Y., Zhang, Y. J., Wang, Y., et al. 2024, GRB Coordinates Network, 37063, 1

Xiao, D., Liu, L.-D., Dai, Z.-G., & Wu, X.-F. 2017, *ApJL*, 850, L41, doi: [10.3847/2041-8213/aa9b2b](https://doi.org/10.3847/2041-8213/aa9b2b)

Xu, F., Huang, Y.-F., Geng, J.-J., et al. 2023, *A&A*, 673, A20, doi: [10.1051/0004-6361/202245414](https://doi.org/10.1051/0004-6361/202245414)

Yamazaki, R., Ioka, K., & Nakamura, T. 2004, *ApJL*, 606, L33, doi: [10.1086/421084](https://doi.org/10.1086/421084)

Yang, H. N., Zhang, W. J., Wang, W. X., et al. 2024a, GRB Coordinates Network, 37188, 1

—. 2024b, GRB Coordinates Network, 37185, 1

Yin, Y.-H. I., Zhang, B.-B., Yang, J., et al. 2024, arXiv e-prints, arXiv:2407.10156, doi: [10.48550/arXiv.2407.10156](https://doi.org/10.48550/arXiv.2407.10156)

Yonetoku, D., Murakami, T., Nakamura, T., et al. 2004, *ApJ*, 609, 935, doi: [10.1086/421285](https://doi.org/10.1086/421285)

Yu, H., Wang, F. Y., Dai, Z. G., & Cheng, K. S. 2015, *ApJS*, 218, 13, doi: [10.1088/0067-0049/218/1/13](https://doi.org/10.1088/0067-0049/218/1/13)

Yuan, W., Zhang, C., Chen, Y., & Ling, Z. 2022, *The Einstein Probe Mission*, ed. C. Bambi & A. Santangelo (Singapore: Springer Nature Singapore), 1–30, doi: [10.1007/978-981-16-4544-0_151-1](https://doi.org/10.1007/978-981-16-4544-0_151-1)

Yuan, W., Zhang, C., Ling, Z., et al. 2024, in *Space Telescopes and Instrumentation 2024: Ultraviolet to Gamma Ray*, ed. J.-W. A. den Herder, S. Nikzad, & K. Nakazawa, Vol. 13093, International Society for Optics and Photonics (SPIE), 130931C, doi: [10.1117/12.3023595](https://doi.org/10.1117/12.3023595)

Zhang, B. 2018, *The Physics of Gamma-Ray Bursts* (Cambridge: Cambridge Univ. Press), doi: [10.1017/9781139226530](https://doi.org/10.1017/9781139226530)

Zhang, B., & Mészáros, P. 2002a, *ApJ*, 571, 876, doi: [10.1086/339981](https://doi.org/10.1086/339981)

—. 2002b, *ApJ*, 581, 1236, doi: [10.1086/344338](https://doi.org/10.1086/344338)

Zhang, B., & Yan, H. 2011a, *ApJ*, 726, 90, doi: [10.1088/0004-637X/726/2/90](https://doi.org/10.1088/0004-637X/726/2/90)

—. 2011b, *ApJ*, 726, 90, doi: [10.1088/0004-637X/726/2/90](https://doi.org/10.1088/0004-637X/726/2/90)

Zhang, F.-W., Shao, L., Yan, J.-Z., & Wei, D.-M. 2012, *ApJ*, 750, 88, doi: [10.1088/0004-637X/750/2/88](https://doi.org/10.1088/0004-637X/750/2/88)

Zhang, W., Woosley, S. E., & MacFadyen, A. I. 2003, *ApJ*, 586, 356, doi: [10.1086/367609](https://doi.org/10.1086/367609)

Zhang, W. J., Shui, Q. C., Wu, H. Z., et al. 2024a, GRB Coordinates Network, 38281, 1

Zhang, W. J., Mao, X., Zhang, W. D., et al. 2024b, GRB Coordinates Network, 35931, 1

Zhang, Y., Geng, J.-J., & Huang, Y.-F. 2019, *ApJ*, 877, 89, doi: [10.3847/1538-4357/ab1b10](https://doi.org/10.3847/1538-4357/ab1b10)

Zhang, Y. J., Liu, M. J., Jiang, S. Q., et al. 2024c, GRB Coordinates Network, 36818, 1

Zhao, X., Li, Z., Liu, X., et al. 2014, *ApJ*, 780, 12, doi: [10.1088/0004-637X/780/1/12](https://doi.org/10.1088/0004-637X/780/1/12)

Zheng, W., Brink, T. G., Filippenko, A. V., et al. 2024, GRB Coordinates Network, 37228, 1

Zhou, H., Chen, W., Sun, H., et al. 2024a, GRB Coordinates Network, 36691, 1

Zhou, H., Wang, W. X., Hu, J. W., et al. 2024b, GRB Coordinates Network, 36997, 1